

Accepted Manuscript

Geological, geochemical and mineralogical characteristics of REE-bearing Las Mercedes bauxite deposit, Dominican Republic

L. Torr3, J.A. Proenza, T. Aiglsperger, T. Bover-Arnal, C. Villanova-de-Benavent, D. Rodr3guez-Garc3a, A. Ram3rez, J. Rodr3guez, L.A. Mosquea, R. Salas

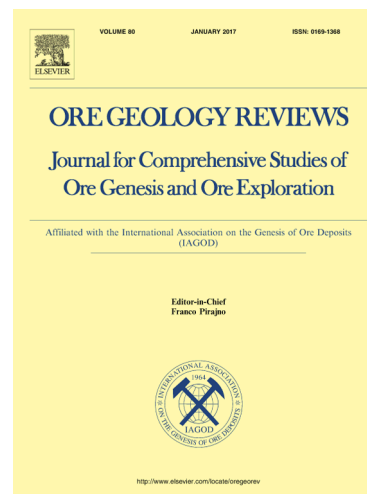
PII: S0169-1368(17)30201-9
DOI: <http://dx.doi.org/10.1016/j.oregeorev.2017.06.017>
Reference: OREGEO 2255

To appear in: *Ore Geology Reviews*

Received Date: 15 March 2017
Revised Date: 7 June 2017
Accepted Date: 12 June 2017

Please cite this article as: L. Torr3, J.A. Proenza, T. Aiglsperger, T. Bover-Arnal, C. Villanova-de-Benavent, D. Rodr3guez-Garc3a, A. Ram3rez, J. Rodr3guez, L.A. Mosquea, R. Salas, Geological, geochemical and mineralogical characteristics of REE-bearing Las Mercedes bauxite deposit, Dominican Republic, *Ore Geology Reviews* (2017), doi: <http://dx.doi.org/10.1016/j.oregeorev.2017.06.017>

This is a PDF file of an unedited manuscript that has been accepted for publication. As a service to our customers we are providing this early version of the manuscript. The manuscript will undergo copyediting, typesetting, and review of the resulting proof before it is published in its final form. Please note that during the production process errors may be discovered which could affect the content, and all legal disclaimers that apply to the journal pertain.



Geological, geochemical and mineralogical characteristics of REE-bearing Las Mercedes bauxite deposit, Dominican Republic

L. Torró^{a,b,*}, J.A. Proenza^a, T. Aiglsperger^a, T. Bover-Arnal^a, C. Villanova-de-Benavent^a, D. Rodríguez-García^a, A. Ramírez^c, J. Rodríguez^c, L.A. Mosquea^b, R. Salas^a

^a Departament de Mineralogia, Petrologia i Geologia Aplicada, Universitat de Barcelona (UB), Martí i Franquès s/n, 08028 Barcelona, Spain

^b Universidad Tecnológica del Cibao Oriental (UTECO), Cotuí, Dominican Republic

^c Servicio Geológico Nacional, Av. Winston Churchill 75, Edificio "J. F. Martínez", Santo Domingo, Dominican Republic

Submitted to Ore Geology Reviews

*Corresponding author: Lisard Torró i Abat

E-mail address: lisardtorro@hotmail.com

Phone: (+34) 934021344

Abstract

Bauxite deposits, traditionally the main source of aluminum, have been recently targeted for their remarkable contents in rare earth elements (REE). With Σ REE (lanthanoids + Sc + Y) concentrations systematically higher than ~ 1400 ppm (av. = 1530 ppm), the Las Mercedes karstic bauxites in the Dominican Republic rank as one of the REE-richest deposits of its style.

The bauxitic ore in the Las Mercedes deposit is mostly unlithified and has a homogeneous-massive lithostructure, with only local cross-stratification and graded bedding. The dominant arenito-roundgrained texture is composed of bauxite particles

and subordinate ooids, pisoids and carbonate clasts. Mineralogically, the bauxite ore is composed mostly of gibbsite and lesser amounts of kaolinite, hematite, boehmite, anatase, goethite, chromian spinel and zircon. Identified REE-minerals include cerianite and monazite-Ce, whose composition accounts for the steady enrichment in light- relative to medium- and heavy-REE of the studied bauxites.

Considering the paleo-geomorphology of the study area, we propose that bauxites in the Las Mercedes deposit are the product of the erosion and deposition of lithified bauxites located at higher elevations in the Bahoruco ranges. Based on the available data, we suggest a mixed lithological source for the bauxite deposits at the district scale: bedrock carbonates and an igneous source of likely mafic composition.

Keywords: karstic bauxite; REE; high tech metals; Dominican Republic

1. Introduction

The European Commission (2014) drew up a list of critical raw materials, namely raw materials that have a high economic importance coupled to a high risk associated with their supply. In that list, the REE (Rare Earth Elements) occupy a prominent position as the raw material with the highest supply risk. According to the International Union of Pure and Applied Chemistry (IUPAC), the REE collective name embraces Sc, Y and lanthanoid (La, Ce, Pr, Nd, Pm, Sm, Eu, Gd, Tb, Dy, Ho, Er, Tm, Yb, Lu) elements (Connelly et al., 2005). Unique electronic, magnetic, optical and catalytic properties make these elements essential in many manufactured alloys and permanent magnets crucial in industrial and defense electronic systems. As such, REE are in the core of the so-called high-tech technologies, which are appointed to play a major role, for instance, in the green energy alternatives to traditional sources (Hatch, 2012; Van Gosen et al., 2014; Weng et al., 2015; Dutta et al., 2016). Although the control of China over the production of REE has decreased significantly over the past 5 years (98% global production in 2010 vs. ~ 85% in the present; Gambogi, 2017), China's monopoly on this commodity likewise is overwhelming. Supply risk and increasing demand are driving governments and mining companies to promote the exploration for REE in a wide variety of *non-conventional* deposit types including sedimentary and residual ones (Chakhmouradian and Wall, 2012; Eliopoulos et al., 2014; Melgarejo, 2015) as well as

“green mining” alternatives focused on their recycling (e.g. Dutta et al., 2016; Ayora et al., 2016).

Laterite (or residual) ores, including bauxite, formed by extensive weathering of a variety of protoliths, are among the most relevant non-conventional deposits for production and benefit of REE. As Wang et al. (2011) put it, “*bauxite and nickel laterite ores are proposed as the most promising scandium resources for its production [sic.]*”. Intense weathering, disintegration of most rock forming minerals and very limited mobility of REE in the weathering environment result in the concentration of these elements relative to their original protoliths, either in secondary REE phases and/or in primary (magmatic) refractory REE-phases and/or adsorbed in residual clays (ion-adsorption clays) (e.g. Mongelli, 1997; Horbe and Costa, 1999; Mordberg, 1999, 2000, 2001; Wang et al., 2000, 2003, 2010; Lanskou and Andreou, 2003; Kynicky et al., 2012; Aiglsperger et al., 2016; Deady et al., 2016). Bauxite deposits, which are currently the main source of aluminum, are classified according to the bedrock lithology as (1) karstic bauxites (overlying carbonate rocks, as in our study case), or as (2) laterite bauxite and (3) Tikhvin types (overlying aluminosilicate rocks) (Bárdossy, 1982). Many karstic bauxite deposits are reported to be relatively enriched in REE (Mongelli, 1997; Mordberg, 1999; Mordberg et al., 2000, 2001; Wang et al., 2003, 2010; Mameli et al., 2007; Eliopoulos et al., 2014; Liu et al., 2016) and often their concentrations are economic as by-products of alumina (Wang et al., 2010; Klyucharev et al., 2013; Deady et al., 2016).

South America and the Caribbean are major bauxite producers and host about the 21% of this resource worldwide (Bray, 2016). In the Greater Antilles of the Caribbean sea, the largest bauxite deposits are located in the central highlands of Jamaica (Nelson et al., 2011). The mineralogy, geochemistry and origin of Jamaican bauxite deposits were mostly published in the 50s to 70s (e.g. Hartman, 1955; Burns, 1961; Waterman, 1962; Hose, 1963; Clarke, 1966; Sinclair, 1967; Comer, 1974). More recently, Wagh and Pinnock (1987) reported significant concentration of REE (e.g., in ppm: 390 Sc₂O₃; 1050 La; 2775 ΣREE) in Jamaican red muds (residue of alumina extraction from bauxite by the Bayer process). Important bauxite reserves exist in Sierra de Bahoruco, SW Dominican Republic. Reserves were initially estimated in 28 MT, with a past production of 4,557,000 tons in the period 1959-1991 by Alcoa Exploration Company

(1959-1983) and Ideal Dominicana (1989-1991) (Nelson et al., 2011). The Las Mercedes deposit, which is located 12 km NE of the town of Pedernales and 185 km WSW of the city of Santo Domingo, is currently the only bauxite deposit under production in the Dominican Republic. The company DOVEMCO resumed production of this deposit in 2013 and reports current reserves of 4,3 MT and an expected operation lifespan of 4 years (Fernández, 2013; DOVEMCO, 2016).

In spite of the growing interest on karstic bauxite deposit as potential, alternative resources of REE and the attested occurrence of important concentration of these elements in Antillean karstic bauxite deposits, the potentiality of Dominican bauxites for the benefit of REE has never been assessed. With that aim in view, we present a detailed petrographic and geochemical characterization of the Las Mercedes deposit, with a particular focus on the REE geochemistry and mineralogy. New data are also used to constraint the origin of bauxite ore in the study area.

2. Geological framework and stratigraphy of the Sierra de Bahoruco

The Sierra de Bahoruco (Bahoruco ranges) in the Bahoruco Peninsula, SW Dominican Republic (Fig. 1A), represents the eastern end of the Presqu'île Du Sud (Southern Peninsula) morphotectonic zone defined by Lewis and Draper (1990). The Sierra de Bahoruco is tectonically limited to the N by the W-E trending Plantain Garden-Enriquillo fault zone; to the E, normal faults associated to the NNE-SSE trending Eastern Beata Ridge Fault sink the mountainous alignment under the Caribbean Sea. Unlike the northern tectonic blocks in Hispaniola, which began to deform in Eocene time in response to the oblique convergence of the North American plate continental margin and the Caribbean island arc (e.g. Mann, 2007; Escuder-Viruete et al., 2006, 2008), the Bahoruco Peninsula block remained apparently undeformed until the Pliocene times (Pérez-Valera, 2010). The collision of the Greater Antilles belt with the Bahamas Platform arrested the northeastward migration of the Caribbean arc, promoted large-scale topographic uplift and changed the regime to the current left-lateral strike-slip tectonics (Mann, 2007). In the Bahoruco Peninsula, associated transpression resulted in overall contractive structures with a conspicuous strike-slip displacement; high-angle reverse and strike-slip faults and soft, km-scale folds accommodated the deformation (Pérez-Valera, 2010). An integrated study of the

sedimentary tectonofacies allowed to Pérez-Valera (2010) to constrain the progressive uplift and shallowing of the Bahoruco ranges from latest Middle Miocene to the present.

The Sierra de Bahoruco is composed of a thick sequence of Eocene to Quaternary carbonates (Figs. 1B-C) with locally well-developed karst systems (de León, 1989; Pérez-Valera, 2010; Pérez-Valera and Abad, 2010). The sedimentary sequence overlies the basaltic Dumisseau Formation (Fig. 1D), which represents the crystalline basement in the area. In Sierra de Bahoruco, the Campanian to lower Eocene volcanic Dumisseau Formation (formerly Río Arriba Formation: de León, 1989) crops out mainly in topographically depressed areas, in the core of regional scale, NW-SE trending anticlines. In the eastern coastal area, the outcrops relate to normal faults aligned broadly parallel to the coastal line. The Dumisseau Formation consists of a sequence of basaltic flows, pyroclastic deposits and much less abundant sedimentary deposits totaling a thickness of at least 1.5 km (Escuder-Viruete, 2010). This formation, which extends westward to the Chaîne de la Serre in S Haiti, is an on-land portion of the Caribbean Large Igneous Province (CLIP) (Lidiak and Anderson, 2015, and references therein). Escuder-Viruete et al. (2016) determined a mantle plume source for the basalts, which are geochemically classified as low-Ti tholeiites, high-Ti transitional basalts and high-Ti and LREE-enriched alkaline basalts.

The carbonate pile in Sierra de Bahoruco records the progressive shift in the environment of deposition from Eocene deep, outer slope, followed by Pliocene shallow, inner platform and reef boundstones, and to Pleistocene emersion (Pérez-Valera, 2010; Pérez-Valera and Abad, 2010). Carbonate materials in the study zone (i.e. in NW Bahoruco Peninsula), listed below, are representative of the whole sedimentary environment progression. We will use here the stratigraphic correlation and nomenclature after Pérez-Valera (2010). Bottom to top, lower Eocene-Oligocene carbonates include (1) the Aceitillar Formation (Fm. lower-middle Eocene), composed of oncolytic massive limestones, (2) local bioclastic loamy limestones of La Compañía Member (Mb.; middle-upper Eocene) and (3) bioclastic limestones of El Mogote Mb. (upper Miocene-lower Oligocene); and the (4) the Neiba Fm. (Eocene-lower Oligocene), composed of micritic, beige-cream in color, limestones containing siliceous. A regional stratigraphic unconformity separates these carbonate units of those of the Upper Oligocene-Miocene. The latter consists of (5) loamy, bioclastic and micritic limestones of the Aguas Negras Unit (upper Oligocene); the Pedernales Unit which

includes (6) the Sitio Nuevo Mb. (Oligocene-lower Miocene) warped limestones and calcarenites, (7) the Loma del Guano Mb. (upper Oligocene-lower Miocene) micritic rosy or beige limestones, (8) the Las Mercedes Mb. (upper Oligocene-middle Miocene) rosy limestones with planktonic foraminifera and (9) the Loma de Peblique Mb. (upper Oligocene-middle Miocene) massive rosy limestones; and (10) the Barahona Unit (middle Miocene-Pliocene?) massive limestones with abundant corals and gastropods. Discordantly overlying are (11) the Pliocene-lower Pleistocene La Cueva Unit reefal, bioclastic limestones. Quaternary (Pleistocene and Holocene) carbonates are linked to lagoon and pocket beach dynamics. The position of the carbonate units and members is synthesized in the stratigraphic column in Fig. 1C.

In the study area, Pleistocene-Holocene decalcification red clays and bauxite argillizations (i.e. materials associated to chemical weathering) are spread in (paleo-) erosion surfaces and karst landforms developed on the Eocene-Pleistocene carbonated sequence (Pérez-Valera, 2010). Repeated Pleistocene-Holocene sea-level highstands associated to fast sea-level oscillations (e.g. Thompson et al., 2011; Moseley et al., 2015) favored the development of important alteration profiles and karsitification (Pérez-Valera, 2010). On the other hand, the progressive and continued uplift of the Batoruco ranges and sea-level lowstands during the same period promoted the erosion of alteration surfaces, transport and deposition in depressed, karstic landforms.

3. Sampling and analytical methods

A total of 23 samples (~1 kg each) were collected at different depths along vertical profiles throughout the mining area.

Major, minor and trace elements of samples were determined at the Actlabs Laboratories (Ontario, Canada) by purchasing the analytical package “4Litho” using fusion inductively coupled plasma emission (FUS-ICP) and inductively coupled plasma emission mass spectrometry (ICP-MS) (for details see <http://www.actlabs.com>).

Twelve samples were selected as the most representative from two bauxite profiles (A and B), eleven consisting of bauxite and one of carbonate. The samples were carefully ground using agate mortar and pestle, and were manually pressed by means of a glass plate to get a flat surface, in cylindrical standard sample holders of 16 millimeters of diameter and 2.5 millimeters of height. The diffractograms were obtained

in a PANalytical X'Pert PRO MPD Alpha1 powder diffractometer in Bragg-Brentano $\theta/2\theta$ geometry of 240 millimeters of radius, nickel filtered Cu K α radiation ($\lambda = 1.5418$ Å), and with 45 kV – 40 mA. During analysis, sample was spun at 2 revolutions per second. A variable divergence slit kept an area illuminated constant (10 mm) and a mask was used to limit the length of the beam (12 mm). Axial divergence Soller slits of 0.04 radians were used. Samples were scanned from 4 to 80° 2 θ with a step size of 0.017° and measuring time of 50 s per step, using a X'Celerator detector (active length = 2.122°). The sample preparation and analysis were performed in the Centres Científics i Tecnològics of the Universitat de Barcelona (CCiT-UB). The software X'Pert HighScore[®] was used to subtract the background of the patterns, to detect the peaks and to assign mineral phases to each peak, as well as to determine semiquantitatively the mineral phases present in the powder samples.

One bauxite sample (i.e. 100 g of homogenized sample) was selected for the production of heavy mineral concentrates at the hydroseparation (HS) laboratory at the University of Barcelona (<http://www.hslab-barcelona.com>) by applying the computer-controlled hydroseparation device CNT HS 11 (Rudashevsky and Rudashevsky, 2007; see also <http://www.cnt-mc.ru>). The proposed methodology for soft rocks by Aiglsperger et al. (2015) was applied. Heavy mineral concentrates from three size fractions (i.e. <30, 30-75, 75-125 μm) were further separated according to their magnetic properties by a FRANTZ magnetic separator. Cylindrical monolayer polished sections (d=2.5 cm) were prepared from each separation product for subsequent investigation.

Mineralogy and textures of bauxites and limestones were studied on 9 polished thin sections, 3 polished sections and 9 monolayer polished sections by means of both transmitted and reflected light petrographic microscopy. Morphological, textural and preliminary compositional features of selected samples were examined by SEM-EDS using an Environmental SEM Quanta 200 FEI, XTE 325/D8395 equipped with an INCA Energy 250 EDS microanalysis system. Operating conditions were an acceleration voltage of 20 kV and a beam current of 1 nA. Chemical analyses of the mineral phases were performed using a JEOL JXA-8230 electron microprobe (EMP) at the CCiT-UB, operated at 20 kV acceleration voltage, 15 nA beam current and with a beam diameter of 5 μm . Analytical standards and lines used for analyses were:

wollastonite (Si K α), apatite (Ca K α , P K α), barite (Ba L α), celestine (Sr L α), UO₂ (U M β), ThO₂ (Th M α), GaAs (Ga L α), YAG (Y L α), LaB₆ (La L α), CeO₂ (Ce L α), REE-1 (Pr L β , Er L α), REE-2 (Ho L β , Tm L α , Eu L α), REE-3 (Yb L α , Sm L β , Gd L α) and REE-4 (Lu L α , Tb L α , Nd L β).

4. Geology of the Las Mercedes deposit

Bauxites of Las Mercedes, the largest deposit in the Bahoruco ranges, cover an area of 2.31 km² and have a rather constant thickness of around 8 to 10 m. The deposit occupies a low-level, peneplain position, and is broadly aligned along the NW-SE trending axis plane of the gentle, regional-scale Las Mercedes syncline (Fig. 1B, D). The deposit presents no sedimentary cover and has a blanket morphology that fills up a huge karst depression developed on bedrock limestones of the Las Mercedes Mb. (Pedernales Unit). The bauxite blanket is only interrupted by random carbonate pillars, corresponding to prominences of the bedrock that protrude from a gentle hummock-shaped to flat base (Fig. 2). High-grade, massive bauxite passes into semi-weathered limestones to the contact with the bedrock limestones and to clayey bauxite or bauxitic clay towards the top (Fig. 3). *Terra rossa* (soft deposit of clay-like appearance, very reddish or brownish-red) covers the karsted surface to a thickness ranging from a few decimeters to two meters.

4.1. Bedrock limestone: textures and facies

Three different facies were recognized in thin sections from samples collected in the Miocene karstified carbonates hosting the bauxite ore of Las Mercedes. The main bedrock facies exhibits wackestone to packstone textures dominated by globigerinids and other planktonic foraminifera (Fig. 4A). The benthic foraminifera of the genus *Nodosaria*, as well as fragments of bivalves, occur. This fossil content indicates a relatively deep, hemipelagic depositional environment. A shallower-water facies characterized by the presence of fragments of colonial corals (Fig. 4B) embedded within a wackestone to packstone matrix, which contains encrusting gypsinid foraminifera, planktonic and benthic foraminifera, coralline algae, peloids and fragments of molluscs and echinoids, was also documented higher up in the succession. The occurrence of fragments of colonial corals indicates a carbonate platform depositional setting. Finally, mudstone textures with scarce tests of the larger foraminifer *Amphistegina*, other

benthic foraminifera and fragments of molluscs and echinoids suggesting more distal platform environments are as well present.

The upper part of the bedrock shows important dissolution features (Fig. 4C) and locally, bauxitic impregnations to a depth of few centimeters. Fractures, dissolution vugs and channels, as well as intra- and interskeletal porosity, are entirely or partly filled with sparry calcite. Skeletal components occurring below the irregular bedrock surface are truncated (Fig. 4B). Locally, the uppermost part of the bedrock corresponds to an authigenic breccia. Accordingly, the Miocene host carbonates underwent ongoing episodes of dissolution and concomitant reprecipitation under subaerial and vadose conditions.

4.2. Bauxitic rock: textures

Bauxites present a homogeneous-massive lithostructure (Fig. 2C, 3B-C), i.e. they are homogeneous in all directions (Bárdossy, 1982), and only subtle, progressive textural changes are observed in the near contact with the bedrock carbonates. Narrow dark red iron-rich crusts of millimeters to few centimeters thick occur at the irregularly-shaped bedrock contact (Fig. 4B); the crusts are made up of an aphanitic matrix with bauxite roundgrains. Above, a pseudobrecciate texture of authigenic origin and an arenite-roundgrained fabric of allothigenic-clastic origin (*sensu* Bárdossy, 1982) mainly form the bauxitic deposits. Laterally out of the bedrock, the bauxite ore becomes unlithified.

The pseudobrecciate texture results from the brecciation of a dark red pelitomorph matrix (Fig. 4D). In such fabrics, fissures that vary in thickness from microns to few millimeters, form dense networks in the aphanitic matrix. Fissuring of the pelitomorph matrix may be related to processes of de-watering (syneresis) or gel compaction (Bárdossy, 1982). Fissures, as well as intergranular pores, are totally or partly filled with sparry calcite. Root traces and fenestrae porosity occluded by blocky calcite also occur. Silt- to sand-sized bauxite particles and roundgrains are common in this texture, as well as mouldic voids of bauxite roundgrains. Scarce ooids occur locally with sizes of less than 0.5 mm in diameter. Ooids have a clastic bauxite particle for nucleus. A complex macropisoid of 2 cm in diameter was also recognized. This single pisoid has a nucleus formed from two micritic carbonate clasts, which occur partly

dissolved (Fig. 5A). Consequently, the pseudobrecciate texture described was also affected by processes of dissolution, reprecipitation and redeposition.

The resedimentation of these bauxite pelitomorphous detritus resulting from the brecciation of the dark red aphanitic matrix documented and of other bauxite deposits gives rise to the arenito-roundgrained texture (Fig. 5B). Accordingly, these bauxite detritus commonly are entirely homogeneous inside. Main textural components correspond to silt- to sand-sized bauxite particles and bauxite roundgrains (up to 1.2 mm in diameter). Subordinate components are ooids (up to 1 mm in diameter) (Fig. 5C), pisoids (up to 1.2 mm in diameter; sensu Bárdossy, 1982), and carbonate clasts, which frequently show dissolution features. Nuclei of ooids correspond to bauxite roundgrains (Fig. 5C) and silt- to sand-sized bauxite particles. Arenito-roundgrained textures locally exhibit cross-stratification (Fig. 5D) and repeated sub-millimetric to centimetric cycles of graded bedding (Fig. 5E). Minor, localized ooidic textures and grainstone fabrics with bedrock-derived calcareous clasts, resedimented fragments of bauxite rocks (Fig. 5F) and coated grains with shell fragments for nucleus occur as well. Small breccias and calcite cements of meteoric and burial origins mainly fill the intergranular space in this texture. Fissures, fenestrae porosity, dissolution vugs and mouldic voids of bauxite roundgrains are normally entirely or partly occluded by sparitic calcite.

5. Mineralogy of the bauxite ore

According to the results obtained by powder X-ray diffraction, gibbsite is the most abundant phase in all the studied samples of both profiles, followed by kaolinite, and minor hematite, boehmite, anatase, chromian spinel and goethite (Figs. 6, 7). The bauxite samples contain variable amounts of gibbsite (29-65 %), and the gibbsite content decreases towards the bedrock (Figs. 6B-D, 7). On the contrary, kaolinite (15-26%), when present, increases towards the bedrock (Figs. 6B-D, 7) so that gibbsite and kaolinite are inversely correlated across the profiles. Hematite, anatase, goethite and chromian spinel are present in all samples across the profiles, always representing less than 15 % of the sample each (Figs. 6, 7). It is worth noting the absence of diasporite and rutile in both profiles. Finally, the bedrock carbonate sample of profile A consists almost entirely of calcite (Fig. 6E). The *terra rossa* samples of profile A contain the lesser amounts of gibbsite (25-29 %) and remarkable amounts of kaolinite (21-23 %), accompanied by quartz (7 %), and the highest boehmite contents (14 %) (Fig. 6A).

Heavy mineral concentrates from bauxite ores contain Fe-Al oxyhydroxide grains (Al-rich goethite?) which occur either as anhedral crystals of sectored plates (Figs. 8A-B) or as rather round-shaped aggregates with variable porosities (Figs. 8C-D). However, these Fe-Al oxyhydroxides are frequently entirely enclosed within Al bearing compounds (Fig. 8E). Small-scaled (<50 μm) subhedral grains of Cr-spinel (Fig. 12F) are rarely observed. In contrast, zircon crystals are fairly abundant within all the investigated size fractions (e.g. Fig. 8G). Zircon grains occur as euhedral to subhedral, stubby to square prismatic crystals, commonly with short pyramidal terminations and aspect ratios of ~ 1.5 to 5 and lengths of ~ 75 to 300 μm . Most zircon grains (i.e. near-entire crystals and fragments) present irregular edges and broken crystal faces most probably due to comminution during transport (Fig. 8G).

The identified REE-phases are cerianite and monazite. Cerianite occurs as replacements, or as coating/impregnating fractures and voids within porous aggregates, of subhedral Fe-Al oxyhydroxide grains (Fig. 8H-I).

Monazite-(Ce) is the main REE-phase in heavy concentrates of bauxite ores from the Las Mercedes deposit. It appears as euhedral to subhedral crystals, ~ 30 to ~ 60 μm across, with isometric-highly modified and less abundant tabular shapes (Fig. 9). Monazite grains exhibit irregular, fractured outlines and other abrasion marks such as scratches, cutouts and notches that evidence turbulent transport. Many crystals host rounded, Si-rich (according to EDS analyses) melt inclusions. Monazite is often found in close relationship with zircon crystals forming mixed grains either sharing a common crystal face or as inclusions of monazite within zircon (Fig. 9). The studied monazite crystals have relatively high and homogeneous ThO_2 (av. = 4.19 wt. %; 0.04 a.p.f.u., normalized to 4 oxygen) and low Ca (av. = 0.81 wt. %) contents (Table 1). The concentrations of BaO, SrO and UO_2 are largely below their detection limits. Cerium (av. = 0.44 a.p.f.u.) is the main REE (Fig. 10), along with less abundant La (av. = 0.25 a.p.f.u.), Nd (av. = 0.14 a.p.f.u.), Sm and Gd (both with av. = 0.04 a.p.f.u.). Most monazite EMP analyses showed analytical totals ~ 100 % and near ideal stoichiometry (both A and B site cations total ~ 1 a.p.f.u.).

6. Geochemistry

6.1. Major and trace element geochemistry and geochemical classification

Whole rock major-, trace- and rare-earth element concentration in samples representative of the bauxitic ore, semi-weathered limestone (close to the contact with the bedrock) and bedrock limestone are given in Table 2. The bauxite samples contain broadly constant high Al_2O_3 (38.57 to 49.34 wt. %), Fe_2O_3 (17.89 to 20.28 wt. %) and TiO_2 (2.03 to 2.61 wt. %) concentrations and erratic amounts of SiO_2 (1.11 to 14.87 wt. %). In the SiO_2 - Al_2O_3 - Fe_2O_3 classification diagram after Bárdossy (1982), bauxites from the Las Mercedes deposit plot broadly along the limit between bauxites *ss* and iron-rich bauxites (Fig. 11). The concentration of alkaline and alkaline earth elements is systematically very low. Low SiO_2 , Fe_2O_3 , and Al_2O_3 , Na_2O and K_2O ($\ll 1$ wt. %) in the bedrock limestone indicate that it contains minor or nil argillite components. Major element concentrations in semi-weathered limestones are intermediate between those in bauxites and bedrock carbonates.

A correlation matrix between the analyzed elements is shown in Appendix A. Strong positive correlations between Al_2O_3 with TiO_2 and Fe_2O_3 (Fig. 12) suggest that they behaved as immobile pairs during the bauxitization process. The positive and negative correlations between Al_2O_3 and SiO_2 at low and high Al_2O_3 concentrations, respectively (Fig. 12), indicate concentration of both elements during initial weathering of the limestones and subsequent depletion of SiO_2 as the Al_2O_3 concentrated during the bauxitization process.

Bauxite samples are enriched in all the analyzed trace elements relative to the semi-weathered limestones, and both lithologies present a conspicuous enrichment relative to the bedrock limestones. The bauxite ores have high contents of V, Ba, Sr, Zr, Cr and Ni, at the level of hundreds of parts per million (ppm). Al_2O_3 yields strong positive correlation with most analyzed trace elements (e.g. Be, V, Cr, Co, Ni, Ga, As, Pb, Th, U). In contrast, the correlation is very poor or absent between Al_2O_3 and Zr, Rb and Cs (Fig. 12). However, the values of Rb and Cs strongly correlate with that of SiO_2 , suggesting that these elements presented equivalent or proportional mobility during bauxitization. The content of Zr is uneven and does not present clear correlation with any other major or trace element.

6.2. REE geochemistry

The studied bauxite samples from the Las Mercedes deposit are steadily enriched in REE to the semi-weathered limestones and both lithologies to the bedrock limestones (Table 2). Bauxite presents systematic high REE contents (Σ REE, including lanthanoids, Sc and Y, ranges between 1389 and 1629 ppm at an average value of 1533 ppm). LREE (La to Eu: 822 to 1008 ppm; av. = 925 ppm) are conspicuously enriched relative to HREE (Gd to Lu: 144 to 167 ppm; av. = 155 ppm), at nearly constant Σ LREE/ Σ HREE ratios (5.5 to 6.6). The concentration of Y is in the range between 361 and 423 ppm (av. = 389 ppm), whereas that of Sc is in the range between 59 to 67 ppm (av. = 64 ppm). Concentrations of individual REE and Σ REE yield strong positive correlations with the Al_2O_3 content, and strong negative correlation with CaO (Fig. 13). The correlation coefficient is systematically equivalent for the Σ LREE and Σ HREE, and hence fractionation of these elements during the bauxitization process is not expected.

Chondrite-normalized REE plot for bauxite, semi-weathered limestone and bedrock limestone samples in Fig. 14 exhibit roughly parallel patterns for the three lithologies. These patterns are characterized by negative slopes as a result of enrichment of the lighter REE relative to medium REE ($\text{La}/\text{Sm}_{\text{CN}}$ between 4.3 and 4.8) and to heavier REE ($\text{La}/\text{Yb}_{\text{CN}}$ between 8.6 and 10.9), and of medium REE to heavy REE ($\text{Gd}/\text{Yb}_{\text{CN}}$ between 1.5 and 1.9). Negative Ce and Eu anomalies are observed in the studied samples from the three lithologies, with Ce/Ce^* and Eu/Eu^* ratios of 0.6 to 1.0 and of 0.6 to 0.9, respectively.

7. Discussion

7.1. Deposit formation and source material of bauxites

Bárdossy (1982) provided an excellent assessment on the theories about the genesis of karstic bauxite deposits to this time, each connected to a contrasting source or parent material from which bauxites formed. Some of these theories have been superseded, but classic elements for discussion remain intact (e.g. Salas et al., 2004; Mameli et al., 2007; Liu et al., 2013). The most widely accepted genetic model ends include (1) latherogenic theories, i.e. bauxite derives from pre-existing laterites developed on aluminosilicate rocks, which are eroded, transported and deposited over a karsted surface; (2) the *terra rossa* theory, i.e. bauxite forms after *terra rossa*, which is the weathering residue of carbonate rocks older than the bauxite; and (3) the volcanogenic theories, i.e. bauxites result from the *in situ* laterization of volcanic ash fallen on the

limestone bedrock. As stressed by Bárdossy (1982), these ends were proposed in origin to account for a salient characteristic of some individual deposits, but a combination of parent rocks are the most plausible scenario for most bauxites instead.

In the study case, the bauxite deposit occupies a peneplain position and is aligned along the axis of a gentle synclinal (Fig. 1B, D). The karsted surface might be visualized as a local synform sedimentary depocenter, which according to Pérez-Valera (2010) was emerged previous to Pleistocene-Holocene times, i.e. previous to the period of bauxite formation. Weathering products of rocks exposed on the surface in the vicinity of the bauxite region could accumulate on the depressed, karsted surface by intermittent streams after great downpours in a tropical climate. Textures and sedimentary structures in studied bauxite samples strongly point to water-borne transport and (re)deposition, and hence the idea of a passive bauxitization limited to the extreme weathering of the bedrock limestone series is ruled out. The scenario of an intense reworking of the bauxite is in agreement with the conspicuous compositional (chemical and mineralogical) homogeneity of the bulk of the bauxite profiles. Clastic dominant components of allothigenic origin including abundant bauxite roundgrains (pebbles) strongly suggest that the Las Mercedes deposit formed after erosion and re-deposition of lithified bauxites; this observation limits the casuistry to an allochthonous or parautochthonous case relative to the karsted area. Under-ore breccia locally developed on semi-weathered bedrock limestones may represent recent karstification after bauxite deposition, as described in Jamaica by Bárdossy (1982); this conclusion harmonizes with chemical and mineralogical trends observed in the near contact with the bedrock limestone.

Several other karstic bauxite deposits are known nearby Las Mercedes, including the Aceitillar deposit, which was completely mined out in the second half of the past century. In Bahoruco, most of the karstic bauxite deposits other than Las Mercedes are hosted in Eocene limestones (Aceitillar Unit; Pérez-Valera, 2010), and are localized in topographically higher areas to the N, NE and E of Las Mercedes (Fig. 1B-D). Therefore, an erosion and water-borne transport from these higher bauxite deposits downhill to the karsted surface in Las Mercedes is reasonable and plausible; the authors champion that the most likely source or parent material for the bauxite ore in Las Mercedes are lithified, older bauxite deposits hosted in limestones of the Aceitillar Unit.

Nevertheless, determining the primeval parent material of bauxites in the Sierra de Bahoruco region as a whole requires consideration of regional potential sources. On the one hand, regional carbonates, semi-weathered limestones and bauxite ore are characterized by similar chondrite-normalized patterns (including tenuous Ce and Eu anomalies; Fig. 14). This observation suggests that regional carbonates might have had an important control on the global REE composition of studied bauxites. On the other hand, the sustained presence of accessory clastic mineral grains of zircon, monazite and chromian spinel (i.e. hard mineral species resistant to weathering and transport) in the studied bauxites indicates contribution of weathered aluminosilicate rocks of igneous origin. That contribution could be either direct or indirect (i.e. eroded from a laterized igneous deposit, including volcanic ash deposits, vs. eroded from laterized sedimentary deposits of volcanogenic origin *sensu* McPhie et al., 1993). As far as the current absence of laterites (of igneous protolith) in the bauxite region does not rule out its former presence and subsequent complete erosion, this option is considered here. In order to constrain the nature of the bauxite igneous parent rocks, the Cr/Zr and the Ti/Cr and Zr/Ti ratios are widely used (e.g. Özlü, 1983; Ordóñez et al., 1990; Mameli et al., 2007). The relatively high Cr contents of the studied bauxite ore result in high Cr/Zr (av. = 4.1) and low Ti/Cr (av. = 26.4) ratios consistent with a mafic parent rock (Özlü, 1983), and so is the Zr/Ti ratio (av. = 0.01; Winchester and Floyd, 1977).

Determining the primeval source material of Bahoruco bauxites is beyond the scope of this article. Nevertheless, on the basis of the above described geological framework for the Bahoruco peninsula, the authors anticipate only two plausible igneous, primeval sources: the crystalline basement, that is basalts of the Campanian-lower Eocene Dumisseau Formation (Pérez-Valera-2010; Escuder-Viruete et al., 2016), and/or volcanic ash fallen on the emerged Eocene-Pliocene carbonate series. It is actually hard to conceive the magmatic crystallization of monazite in the Dumisseau basalts, and this mineral was not described by Escuder-Viruete et al. (2016); nevertheless, the LREE enrichment of high-Ti transitional and alkaline basalts of the Dumisseau Formation (Fig. 14) would account for the LREE enrichment relative to HREE in the bauxite ore. As for the volcanic ash, quaternary alkaline basaltic volcanism is described across the south-central Hispaniola, apparently associated to the strike-slip tectonic activity along the Enriquillo-Plantain Garden Fault Zone (Fig. 1A) (Kamenov et al., 2011; Lidiak and Anderson, 2015). Accordingly, volcanic activity occurred just north of the Bahoruco

region at the time bracketed for the bauxite formation. Wind-borne volcanic ash fallen on a karst surface was proposed as source material of Jamaican bauxites (Waterman, 1962; Comer, 1974). In order to accurately discern the primeval source material from which bauxites formed in Bahoruco, further work from a larger set of samples including other bauxite ores from the region, and zircon and monazite dating, is needed.

7.2. Rare Earth Element resources

Studied bauxite samples from the Las Mercedes deposit present Σ REE systematically above ~ 1400 ppm and an average value of ~ 1530 ppm ($n=15$). These figures place Las Mercedes in the top ranking of REE-enriched karstic bauxite deposits worldwide. The highest Σ REE values given by Wang et al. (2010) for the Quyang bauxite deposit in China are comparable, but the reported REE values are highly erratic from sample to sample (233 to 1992 ppm; av. = 692 ppm). Also erratic are the Σ REE concentrations in other bauxites from China such as the Guandou deposit (84 to 1306 ppm, av. = 627 ppm; Liu et al., 2013) and those in western Guangxi (100 to 4491 ppm, av. = 610; Liu et al., 2016), the Schugorsk deposit in Russia (206 to 3009 ppm, av. = 1062 ppm; Mordgerg et al., 2001) and bauxites from Nurra, Italy (56 to 2888 ppm; av. = 496 ppm; Mameli et al., 2007). In bauxite deposits from the Zagros Mountain Belt in Iran, Zarasvandi et al. (2008) report Σ REE values up to 730 ppm. Σ REE concentration in the Las Mercedes ore is higher than average Σ REE concentrations in red mud wastes in Parnassus-Giona (Greece; Σ REE from 728 to 790 ppm, av. = 767 ppm) and Seydişehir (Turkey; Σ REE from 133 to 1777 ppm, av. = 989 ppm), obtained after processing a bauxite feed with Σ REE 646 and 446 ppm (av. values), respectively (Deady et al., 2016, and references therein). In Jamaican red mud ponds, Σ REE concentrations are commonly above 2000 ppm (up to 2775 ppm) after the processing of a bauxite feed with maximum Σ REE of 1075 ppm (Wagh and Pinnock, 1987).

According to Bao and Zhao (2008), concentrations of only 500 ppm in weathering crusts over granitic rocks are suitable for the processing of REE; average Σ REE in the Las Mercedes ore triples this figure. Bauxitic ores, in addition, offer a series of advantages such as huge tonnages and easiness to concentrate that make it appealing over other mineralization styles (e.g. Klyucharev et al., 2013). Likewise, the geometry of the Las Mercedes deposit allows its exploitation by simple open pit mechanical rock excavation by means of a bucket.

As it appears from above, red muds, which are the waste after alumina extraction from bauxite ores by the Bayer process, commonly double or triple the Σ REE concentration of the original ores. Therefore, by-product production of REE from bauxite can be envisaged as a sequenced, two-step flowsheet including (1) the extraction of alumina from a bauxite feed by means of the Bayer process, and (2) extraction of REE from a red mud feed. This approach safeguards the production of alumina.

The extraction of REE from red muds has been increasingly tested and upgraded during the last decade and Borra et al. (2010) describes an extraction of ~ 80 % REE as a result of simple acid leaching. These rates can be further improved by a combined sulfation-roasting-leaching process designed to address the problem of iron dissolution, ideal for iron-rich bauxite ores such as Las Mercedes (Borra et al., 2016). The effectiveness and profitability of the REE extraction process will strongly depend also on the mineralogical expression of REE and other metals in the red muds (Deady et al., 2016, and references therein). Monazite is the main REE-phase found in the Las Mercedes bauxite ore, along with less abundant cerianite. Processing techniques for the extraction of REE from monazite are quite well and long understood (e.g. Crouse and Brown, 1959). Interestingly, recent reviews (e.g. Kumari et al., 2015) coincide to propose a thermal treatment (roasting) previous to acid leaching for the recovery of REE from monazite concentrates, which concurs indeed with the flowsheet proposed by Borra et al. (2016) for the recovery of REE from a red mud, all-in-one feed (i.e., on paper, a previous concentration of monazite would not be necessary).

8. Conclusions

Bauxite ore mined in the Las Mercedes deposit, Dominican Republic, is characterized by relatively high and homogeneous concentrations of REE, with Σ REE systematically above 1400 ppm and averaging 1530 ppm. These figures place that deposit as one of the richest bauxite deposits worldwide with regards to these elements. Identified REE-phases are cerianite and Th-rich monazite-(Ce). Bauxite ore of Las Mercedes might be by-products or coproducts during the production of Al.

Las Mercedes deposit likely formed after erosion and re-deposition of lithified bauxites located at higher elevations in the Bahoruco ranges. On the origin of bauxites

in the Sierra de Bahoruco region as a whole, weathering of regional carbonates could be a significant participant along with a conspicuous contribution of an igneous source of likely mafic composition.

Acknowledgments

This research has been funded by the project 2014-1B4-133 of the *Ministerio de Educación, Ciencia y Tecnología* of the Dominican Government and the Catalan projects 2014-SGR-1661 and 2014-SGR-251, and received support for analyses at the *Serveis Científics i Tecnològics* from the University of Barcelona. The help and hospitality extended by the DOVEMCO staff, driver Wilson and assistants Jonhy and Lily during fieldwork are also gratefully acknowledged, as well as the technical support in EMP sessions by Dr. X. Llovet. Ideas on the source material of Las Mercedes bauxite greatly benefited from discussion with J. Escuder-Viruete about the regional geology. We are grateful to two anonymous reviewers for their accurate reviews and to Dr. F. Pirajno for the competent editorial handling.

References

- Aiglsperger, T., Proenza, J.A., Zaccarini, F., Lewis, J.F., Garuti, G., Labrador, M., Longo, F., 2015. Platinum group minerals (PGM) in the Falcondo Ni laterite deposit, Loma Caribe peridotite (Dominican Republic). *Miner. Deposita* 50, 105–123.
- Aiglsperger, T., Proenza, J.A., Lewis, J.F., Labrador, M., Svojtka, M., Rojas-Purón, A., Longo, F., Durišová, J., 2016. Critical metals (REE, Sc, PGE) in Ni-laterites from Cuba and the Dominican Republic. *Ore Geol. Rev.* 73, 127–147.
- Ayora, C., Macías, F., Torres, E., Lozano, A., Carrero, S., Nieto, J.M., Pérez-López, R., Fernández-Martínez, A., Castillo-Michel, H., 2016. Recovery of Rare Earth Elements and Y from Passive-Remediation Systems of Acid Mine Drainage. *Environmental Science and Technology* 50, 8255–8262.
- Bao, Z., Zhao, Z., 2008. Geochemistry of mineralization with exchangeable REY in the weathering crusts of granitic rocks in South China. *Ore Geol. Rev.* 33, 519–535.
- Bárdossy, G., 1982. Karst bauxites. Bauxite deposits on carbonate rocks, *Developments in Economic Geology*, 14. Elsevier, Budapest.
- Borra, C.R., Pontikes, Y., Binnemans, K., Gerven, T.V., 2010. Leaching of rare earths from bauxite residue (red mud). *Miner. Eng.* 76, 20–27.

- Borra, C.R., Mermans, J., Blanpain, B., Pontikes, Y., Binnemans, K., Gerven, T.V., 2016. Selective recovery of rare earths from bauxite residue by combination of sulfation, roasting and leaching. *Miner. Eng.* 92, 151–159.
- Boynton, W.V., 1985. Chapter 3: Cosmochemistry of the rare earth elements: Meteorite studies, in: Henderson, P. (Ed.), *Rare Earth Element Geochemistry*, (Developments in Geochemistry 2), Elsevier, Amsterdam.
- Bray, E.L., 2016. Mineral Commodity Summaries: Bauxite and Alumina. USGS <http://minerals.usgs.gov/minerals/pubs/commodity/bauxite/mcs-2016-bauxi.pdf> (accessed 10.07.2016).
- Burns, D.J., 1961. Some chemical aspects of bauxite genesis in Jamaica. *Econ. Geol.* 56, 1297–1303.
- Chakhmouradian, A.R., Wall, F., 2012. Rare Earth Elements: Minerals, Mines, Magnets (and more). *Elements* 8, 333–340.
- Clarke, O.M., 1966. The formation of bauxite on karst topography in Eufaula District, Alabama and Jamaica, West Indies. *Econ. Geol.* 61, 903–916.
- Comer, J.B., 1974. Genesis of Jamaican bauxite. *Econ. Geol.* 69, 1251–1264.
- Connelly, N.G., Damhus, T., Harsthor, R.M., Hutton, A.T., 2005. Nomenclature of Inorganic Chemistry: IUPAC recommendations. International Union of Pure and Applied Chemistry, Cambridge.
- Crouse, D.J., Brown, B., 1959. Recovery of thorium, uranium and rare earths from monazite sulfate liquors by the amine extraction (AMEX) process. OAK Ridge National Laboratory, Tennessee.
- Deady, E.A., Mouchos, E., Goodenough, K., Williamson, B.J., Wall, F., 2016. A review of the potential for rare-earth element resources from European red muds: examples from Seydişehir, Turkey and Parnassus-Giona, Greece. *Mineral. Mag.* 80, 43–61.
- de León, O., 1989. Geología de la Sierra de Bahoruco (República Dominicana). Museo Nacional de Historia Natural, Santo Domingo.
- DOVEMCO, 2016. Operaciones, Bauxita de Pedernales. <http://www.dovemco.com.do/nosotros/otras-paginas/bauxita> (accessed 12.07.2016).
- Dutta, T., Kim, K.-H., Uchimiya, M., Kwon, E.E., Jeon, B.-H., Deep, A., Yun, S.-T., 2016. Global demand for rare earth resources and strategies for green demand. *Environ. Res.* 150, 182–190.
- Eliopoulos, D., Economou, G., Tzifas, I., Papatrechis, C., 2014. The potential of Rare Earth Elements in Greece. European Rare Earth Resources Conference, Proceedings, 308–316.

- Escuder-Viruete, J., 2010. Mapa Geológico de la República Dominicana E. 1:50.000. Informe (Parte 1) de Petrología de Rocas Ígneas y Metamórficas, Hojas de Polo, La Ciénaga, Enriquillo, Sabana Buey y Nizao. Dirección General de Minería, Santo Domingo.
- Escuder-Viruete, J., Contreras, F., Stein, G., Urien, P., Joubert, M., Ullrich, T., Mortensen, J., Pérez-Estaún, A., 2006. Transpression and strain partitioning in the Caribbean Island-arc: Fabric development, kinematics and Ar-Ar ages of syntectonic emplacement of the Loma de Cabrera batholith, Dominican Republic. *J. Struct. Geol.* 28, 1496–1519.
- Escuder-Viruete, J., Joubert, M., Urien, P., Friedman, R., Weis, D., Ullrich, T., Pérez-Estaún, A., 2008. Caribbean island-arc rifting and back-arc basin development in the Late Cretaceous: Geochemical, isotopic and geochronological evidence from Central Hispaniola. *Lithos* 104, 378–404.
- Escuder-Viruete, J., Joubert, M., Abad, M., Pérez-Valera, F., Gabites, J., 2016. The basaltic volcanism of the Dumisseau Formation in the Sierra de Bahoruco, SW Dominican Republic: A record of the mantle plume-related magmatism of the Caribbean Large Igneous Province. *Lithos* 254–255, 67–83.
- European Commission, 2014. Report on critical raw materials for the EU; Report of the Ad hoc Working Group on defining critical raw materials. <http://ec.europa.eu/DocsRoom/documents/10010/attachments/1/translations/en/renditions/native> (accessed 10.07.2016).
- Fernández, H., 2013. Explotación actual de la bauxita en la Sierra de Bahoruco. Libro de Resúmenes del 2º Congreso Dominicano de Geología, 43.
- Gambogi, J., 2017. Rare Earths. U.S. Geological Survey, Mineral Commodity Summaries, pp. 134–135.
- Hartman, J.A., 1955. Origin of heavy minerals in Jamaican bauxite. *Econ. Geol.* 50, 738–747.
- Hatch, G.P., 2012. Dynamics in the Global Market for Rare Earths. *Elements* 8, 341–346.
- Horbe, A., Costa, M., 1999. Geochemical evolution of a lateritic Sn–Zr–Th–Nb–Y–REE bearing ore body derived from apogranite: the case of Pitinga, Amazonas-Brazil. *J. Geochem. Explor.* 66, 339–351.
- Hose, H.R., 1963. Jamaica type bauxites developed on limestones. *Econ. Geol.* 58, 62–69.
- Kamenov, G.D., Perfit, M.R., Lewis, J.F., Gross, A.R., Arévalo, R., Shuster, R.D., 2011. Ancient lithospheric source for Quaternary lavas in Hispaniola. *Nat. Geosci.* 4, 554–557.
- Klyucharev, D.S., Volkova, N.M., Comyn, M.F., 2013. The problems associated with using non-conventional rare-earth minerals. *J. Geochem. Explor.* 133, 138–148

- Kumari, A., Panda, R., Jha, M.K., Kumar, J.R. and Lee, J.Y., 2015. Process development to recover rare earth metals from monazite mineral: A review. *Miner. Eng.* 79, 102–115.
- Kynicky, J., Smith, M.P., Xu, C., 2012. Diversity of Rare Earth Deposits: The Key Example of China. *Elements* 8, 361–367.
- Laskou, M., Andreou, G., 2003. Rare earth elements distribution and REE-minerals from the Parnassos–Ghiona bauxite deposits, Greece, in: Eliopoulos, D., et al. (Eds.), *Mineral Exploration and Sustainable Development, 7th Biennial SGA Meeting*, Athens. Mill Press, Rotterdam.
- Lewis, J.F., Draper, G., 1990. Geology and tectonic evolution of the Northern Caribbean margin, in: Dengo, G., Case, J.E. (Eds.), *The Caribbean region*. Boulder, Colorado, Geol. Soc. Am., *The Geology of North America H*, 77–140.
- Lidiak, E.G., Anderson, T.H., 2015. Evolution of the Caribbean plate and origin of the Gulf of Mexico in light of plate motions accommodated by strike-slip faulting, in: Anderson, T.H., Didenko, A.N., Johnson, C.L., Khanchuk, A.I., MacDonald, J.H., Jr. (Eds.), *Late Jurassic Margin of Laurasia-A Record of Faulting Accommodating Plate Rotation*. Geological Society of America Special Paper 513, SPE513–01.
- Liu, X., Wang, Q., Feng, Y., Li, Z., Cai, S., 2013. Genesis of the Guangou karstic bauxite deposit in western Henan, China. *Ore Geol. Rev.* 55, 162–175.
- Liu, X., Wang, Q., Zhang, Q., Zhang, Y., Li, Y., 2016. Genesis of REE minerals in the karstic bauxite in western Guangxi, China, and its constraints on the deposit formation conditions. *Ore Geol. Rev.* 75, 100–115.
- Mameli, P., Mongelli, G., Oggiano, G., Dinelli, E., 2007. Geological, geochemical and mineralogical features of some bauxite deposits from Nurra (Western Sardinia, Italy): insights on conditions of formation and parental affinity. *Int. J. Earth Sci.* 96, 887–902.
- Mann, P., 2007. Overview of the tectonic history of northern Central America. *Geol. S. Am. S.* 428, 1–19.
- McPhie, J., Doyle, M., Allen, R., 1993. *Volcanic textures: a guide to the interpretation of textures in volcanic rocks*. Centre for Ore Deposits and Exploration Studies, University of Tasmania, Hobart.
- Melgarejo, J.C., 2015. Rare earth elements: conventional and non-conventional deposits. *Seminarios de la Sociedad Española de Mineralogía*, 10 (in press).
- Mongelli, G., 1997. Ce-anomalies in the textural components of Upper Cretaceous karst bauxites from the Apulian carbonate platform (southern Italy). *Chem. Geol.* 140, 69–79.
- Mordberg, L.E., 1999. Geochemical evolution of a Devonian diaspore–crandallite–svanbergite-bearing weathering profile in the Middle Timan, Russia. *J. Geochem. Explor.* 66, 353–361.

- Mordberg, L.E., Stanley, C.J., Germann, K., 2000. Rare earth element anomalies in crandallite group minerals from the Schugorsk bauxite deposit, Timan, Russia. *Eur. J. Mineral.* 12, 1229–1243.
- Mordberg, L.E., Stanley, C.J., Germann, K., 2001. Mineralogy and geochemistry of trace elements in bauxites: the Devonian Schugorsk deposit, Russia. *Mineral. Mag.* 65, 81–101.
- Moseley, G.E., Richards, D.A., Smart, P.L., Standish, C.D., Hoffmann, D.L., Hove, H., Vinn, O., 2015. Early–middle Holocene relative sea-level oscillation events recorded in a submerged speleothem from the Yucatán Peninsula, Mexico. *Holocene* 25, 1511–1521.
- Nelson, C.E., Proenza, J.A., Lewis, J.F., Lopez-Kramer, J., 2011. The metallogenic evolution of the Greater Antilles. *Geol. Acta* 9, 229–264.
- Ordóñez, S., Fort, R., Bustillo, M., 1990. Estudio de las tierras raras en las bauxitas kársticas del noreste de la Península Ibérica. *Estudios geológicos* 46, 373–384.
- Özlu, N., 1983. Trace-element content of karst-bauxites and their parent rocks in the Mediterranean Belt. *Miner. Deposita* 18, 469–476.
- Pérez-Valera, F., 2010. Geologic Map Sheet 1:50.000 num. 5970-III and corresponding memoir. Proyecto 1B de Cartografía Geotemática de la República Dominicana. Programa SYSMIN. Dirección General de Minería, Santo Domingo.
- Pérez-Valera, F., Abad, M., 2010. Informe Estratigráfico y Sedimentológico. Proyecto 1B de la Cartografía Geotemática de la República Dominicana. Programa SYSMIN. Dirección General de Minería, Santo Domingo.
- Rudashevsky, N.S., Rudashevsky, V.N., 2007. Patent of Russian Federation #69418, industrial (useful) model, “Device for separation of solid particles”, Moscow, December 27, 2007.
- Salas, R., Vaquer, R., Travé, A., 2004. Bauxitas kársticas y arcillas lateríticas barreñenses de la Cadena Ibérica oriental y la Cadena Costera Catalana: relaciones genéticas y áreas de procedencia. *Geo-temas* 6, 123–126.
- Sinclair, I.G.L., 1967. Bauxite genesis in Jamaica: new evidence from trace element distribution. *Econ. Geol.* 62, 482–486.
- Thompson, W.G., Curran, H.A., Wilson, M.A., White, B., 2011. Sea-level oscillations during the last interglacial highstand recorded by Bahamas corals. *Nat. Geosci.* 4, 684–687.
- Van Gosen, B.S., Verplanck, P.L., Long, K.R., Gambogi, Joseph, Seal, R.R., II, 2014, The rare-earth elements—Vital to modern technologies and lifestyles: U.S. Geological Survey Fact Sheet 2014–3078, <http://dx.doi.org/10.3133/fs20143078>.
- Wagh, A.S., and Pinnock, W.R., 1987. Occurrence of scandium and rare earth elements in Jamaican bauxite waste. *Econ. Geol.* 82, 757–761.

- Wang, Y.X., Li, H.M., Yang, J.D., Qiu, L.W., Chai, D.H., Chen, P., 2000. Discovery of paleoweathering type rare and rare earth element deposits in Northern China and its significance. *Geological Journal of China Universities* 6, 605–607.
- Wang, Y.X., Li, H.M., Yang, J.D., Shen, Y.Q., Chai, D.H., Chen, P., Qiu, L.W., Chen, X.M., Zhao, L.X., Zhu, C., Ge, J.J., 2003. Palaeoweathering type rare earth element deposit in Shanxi determined by solid isotope mass spectrometry. *Journal of Chinese Mass Spectrometry Society* 24, 394–397.
- Wang, Q.F., Deng, J., Liu, X.F., Zhang, Q.Z., Sun, S., Jiang, C.Z., Zhou, F., 2010. Discovery of the REE minerals and its geological significance in the Quyang bauxite deposit, West Guangxi, China. *J. Asian Earth Sci.* 39, 701–712.
- Wang W., Pranolo Y., Cheng C.Y., 2011. Metallurgical processes for scandium recovery from various resources: A review. *Hydrometallurgy* 108, 100–108.
- Waterman, G.C., 1962. Some chemical aspects of bauxite genesis in Jamaica. *Econ. Geol.* 57, 829–830.
- Weng, Z., Jowitt, S.M., Mudd, G.M., Haque, N., 2015. A Detailed Assessment of Global Rare Earth Element Resources: Opportunities and Challenges. *Econ. Geol.* 110, 1925–1952.
- Winchester, J.A., Floyd, P.A., 1977. Geochemical discrimination of different magma series and their differentiation products using immobile elements. *Chem. Geol.* 20, 325–343.
- Zarasvandi, A., Charchi, A., Carranza, E.J.M., Alizadeh, D., 2008. Karst bauxite deposits in the Zagros Mountain Belt, Iran. *Ore Geol. Rev.* 34, 521–532.

Table and figure captions

Table 1. Representative EMP analyses of monazite crystals from the Las Mercedes bauxite deposit. Cations normalized to 4 O.

Table 2. Major, trace and rare earth element compositions of analyzed bauxite, semi-weathered limestone and bedrock limestone samples from the Las Mercedes deposit.

Figure 1. (A) Map of the Hispaniola Island showing the location of the studied area and the main fault systems (EPGFZ: Enriquillo-Plantain Garden Fault Zone; SJRFZ: San Juan Restauración; BGFZ: Bonao-La Guácara; HFZ: Hispaniola; SFZ: Septentrional). (B) Geologic map of the studied area (modified from Pérez-Valera, 2010) with the location of the Las Mercedes bauxite deposit (A). (C) Schematic lithostratigraphic

column of carbonates in the studied area showing the location of the Las Mercedes bauxite deposit (A). (D-D') Cross section of the studied area, slightly modified from Pérez-Valera (2010), showing the location of the Las Mercedes bauxite deposit in the edge of the Las Mercedes anticline; the location of the cross section is shown in B.

Figure 2. Field photographs of the Las Mercedes open pit mine. (A) General view of the deposit with the mined out portion (and remaining limestone columns) in the front and the active pit face to the background of the image. (B) The white carbonate columns stand out against the deep-red bauxite; after stripping of topsoil, mining progresses by scrapping off the friable, massive bauxite with an excavator bucket. (C) View of the active pit face; note the massive texture of high-grade bauxite and the rather constant thicknesses of about 10 m.

Figure 3. (A) Representative specimen of semi-weathered limestone picked up close to the contact with the bauxite ore. (B) Detail of the massive texture that characterize the bauxite ore in the Las Mercedes deposit. (C) Isolated Fe oxyhydroxide concretion floating in massive bauxite; the nodule is 3 mm across. (D) *Terra rossa* and soil terrace to the top of the bauxite ore and karsted surface.

Figure 4. Photomicrographs of bedrock and bauxite textures and components. (A) Detail of a bedrock wackestone texture containing abundant globigerinids and other planktonic foraminifera. White arrow points to a test of *Nodosaria* benthic foraminifera. (B) Close-up view of the contact (yellow discontinuous line) between the bedrock, which exhibits a truncated fragment of a coral colony, and the bauxitic rock. Note the irregular shape exhibited by the contact resulting from dissolution processes, and the iron-rich crust above. (C) Detail of the highly irregular karstic surface (blue discontinuous line) exhibited by the limestone bedrock and the overlying bauxitic deposits. (D) Example of a pseudobrecciate texture resulting from the brecciation of a dark red pelitomorph matrix. Note the dense irregular network of fissures.

Figure 5. Photomicrographs of bauxite textures and components. (A) Close-up view of a composite macropisoid with a nucleus formed from two partly dissolved micritic carbonate clasts. (B) Example of an arenito-roundgrained texture. Bauxite grains occur cemented by blocky calcite. Note the graded bedding displayed by the bauxite roundgrains. Partly dissolved bauxite particles and mouldic voids of bauxite

roundgrains are indicated with yellow arrows. (C) Close-up view of an ooid present in the bauxite rock examined. (D) Detail of oblique stratification exhibited by the arenite-roundgrained texture. (E) Close-up view of repeated sub-millimetric to centimetric cycles of graded bedding. (F) Clastic bauxite grains cemented by sparry calcite that indicate repeated reworking of bauxite deposits.

Figure 6. Selected X-ray diffractograms of the profile A from the Las Mercedes bauxite deposit, from the carbonate bedrock to the upper, highly weathered, bauxitic levels: (A) sample M-P6-1 (*terra rossa*), (B) M-P1-1 (bauxite far from the bedrock limestone), (C) M-P1-3 (bauxite), (D) M-P1-6 (bauxite close to the bedrock limestone), (E) M-P1-5 (bedrock carbonate). Abbreviations: Ant (anatase), Bhm (boehmite), Chr (chromian spinel), Gbs (gibbsite), Gth (goethite), Hem (hematite), Kln (kaolinite), Qz (quartz).

Figure 7. Pie diagrams representing the semiquantitative results obtained by powder X-ray diffraction in profile A (A) and profile B (B). The position of the samples is depicted in the corresponding field photographs.

Figure 8. SEM-BSE photomicrographs of grains in dense concentrates after hydroseparation including Fe-Al oxyhydroxide (A-E, H-I), chromian spinel (F) and zircon (G) grains. In H and I, cerianite occurs as replacement of porous aggregates of Fe-Al oxyhydroxides.

Figure 9. SEM-BSE photomicrographs of monazite grains from the Las Mercedes deposit with isometric (A, D, E) and tabular (B) shapes. Fractured outlines (A) and scratches and notches (B) are common. Many grains host melt inclusions (C, D). (E) Mixed monazite-zircon grain with close intergrowth between the two phases. (F) Monazite inclusion within a zircon grain. Mnz=monazite; Zrn=zircon.

Figure 10. Triangular plots of the REE compositions of analyzed monazite crystals from the Las Mercedes bauxite deposit. Note that Ce is the dominant REE along with less abundant La, and that the concentration of the other REE and Th is remarkably lower.

Figure 11. Whole rock Al_2O_3 - SiO_2 - $\text{Fe}_2\text{O}_3(\text{t})$ ternary plot of studied bauxites and semi-weathered limestones; bauxite classification fields are after Bárdossy (1982).

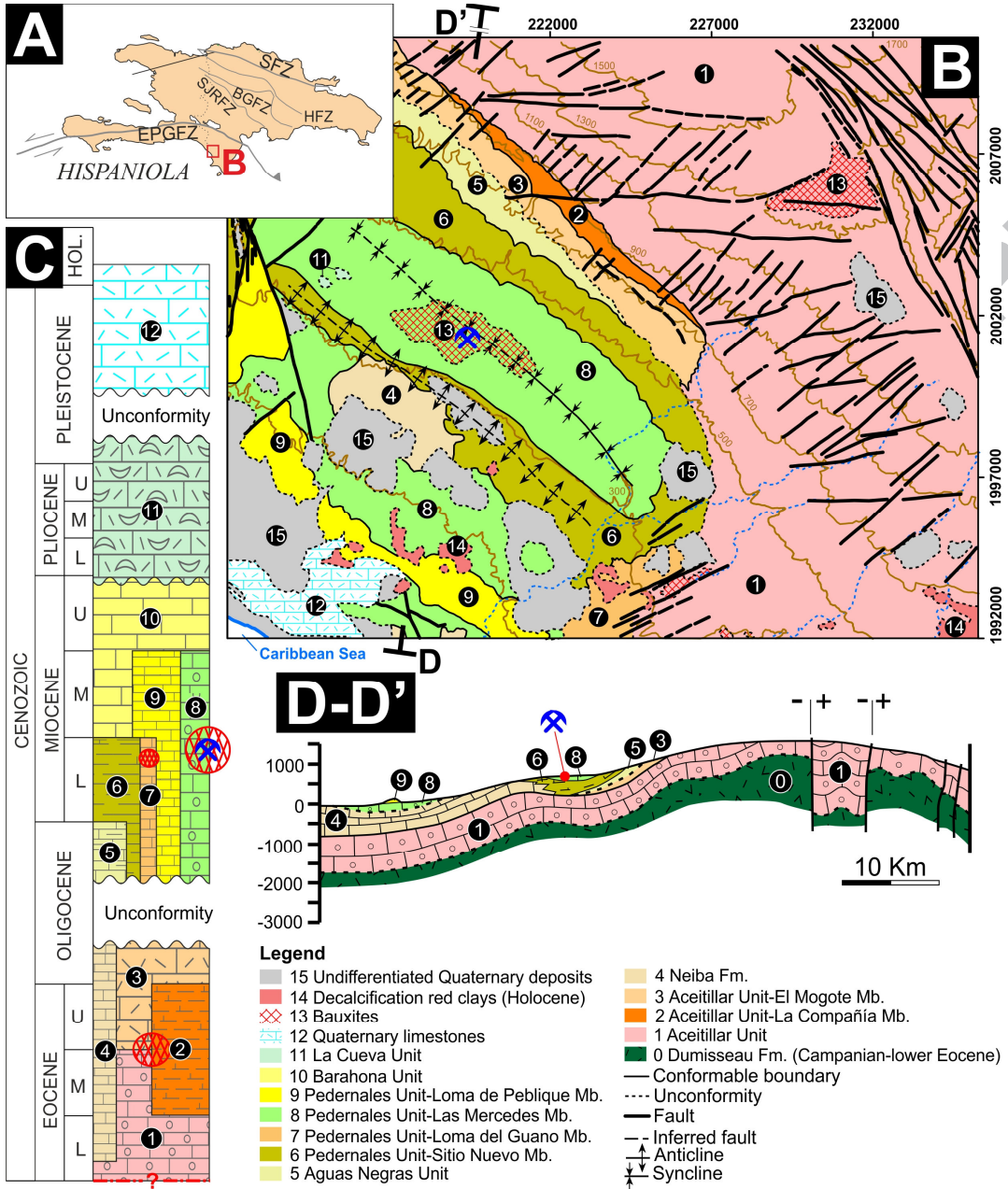
Figure 12. Selected bivariate whole rock major- and trace-element diagrams for bauxites, semi-weathered limestones and bedrock limestones, and inferred trends (red arrows) during the bauxitization process. For further details, see the main text.

Figure 13. Whole rock ΣREE vs. Al_2O_3 and ΣREE vs. CaO bivariate diagrams for bauxites, semi-weathered limestones and bedrock limestones from the Las Mercedes deposit.

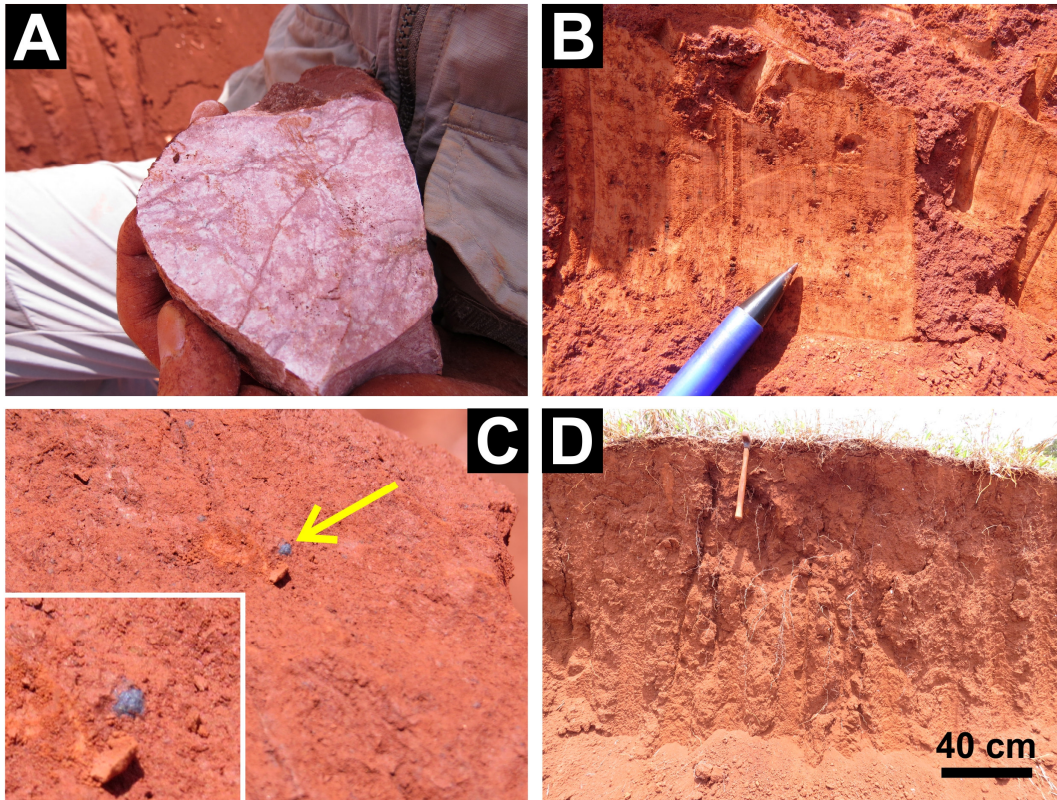
Figure 14. Chondrite-normalized REE plot for whole rock data of studied bauxite, semi-weathered limestone and bedrock limestone samples. Normalization values are after Boynton (1985). The whole rock geochemical data for the Dumisseau Formation lithotypes is from Escuder-Viruete et al. (2016).

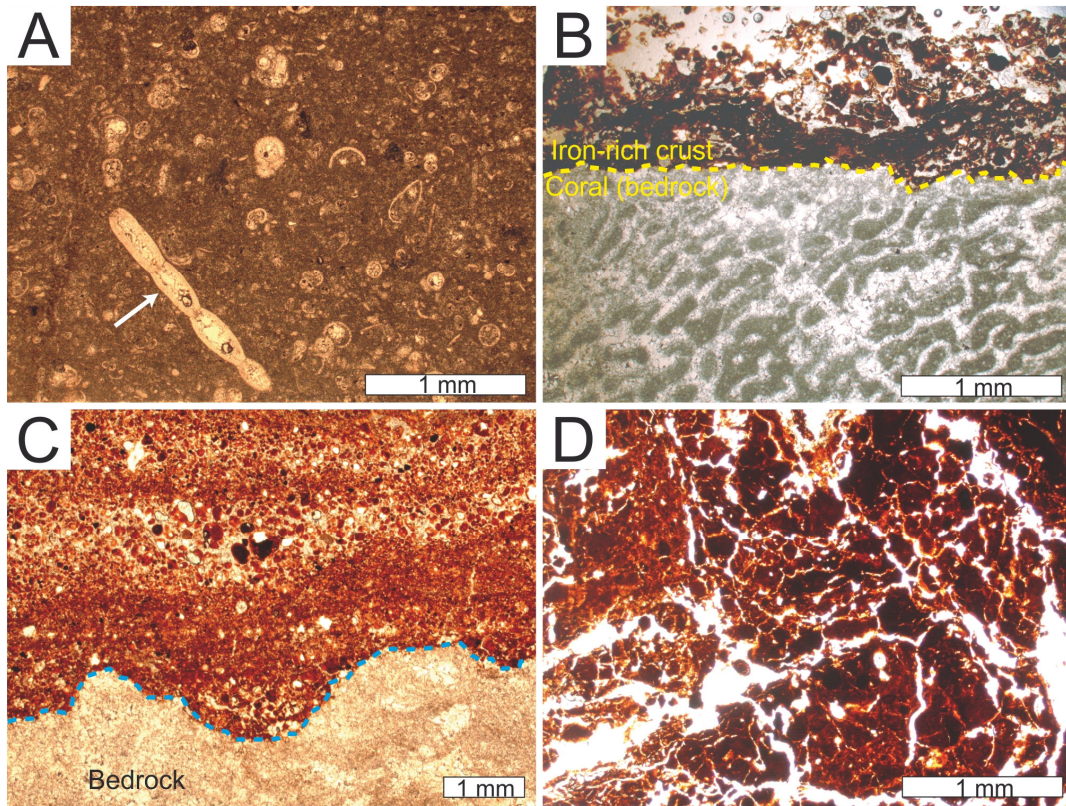
Annexes

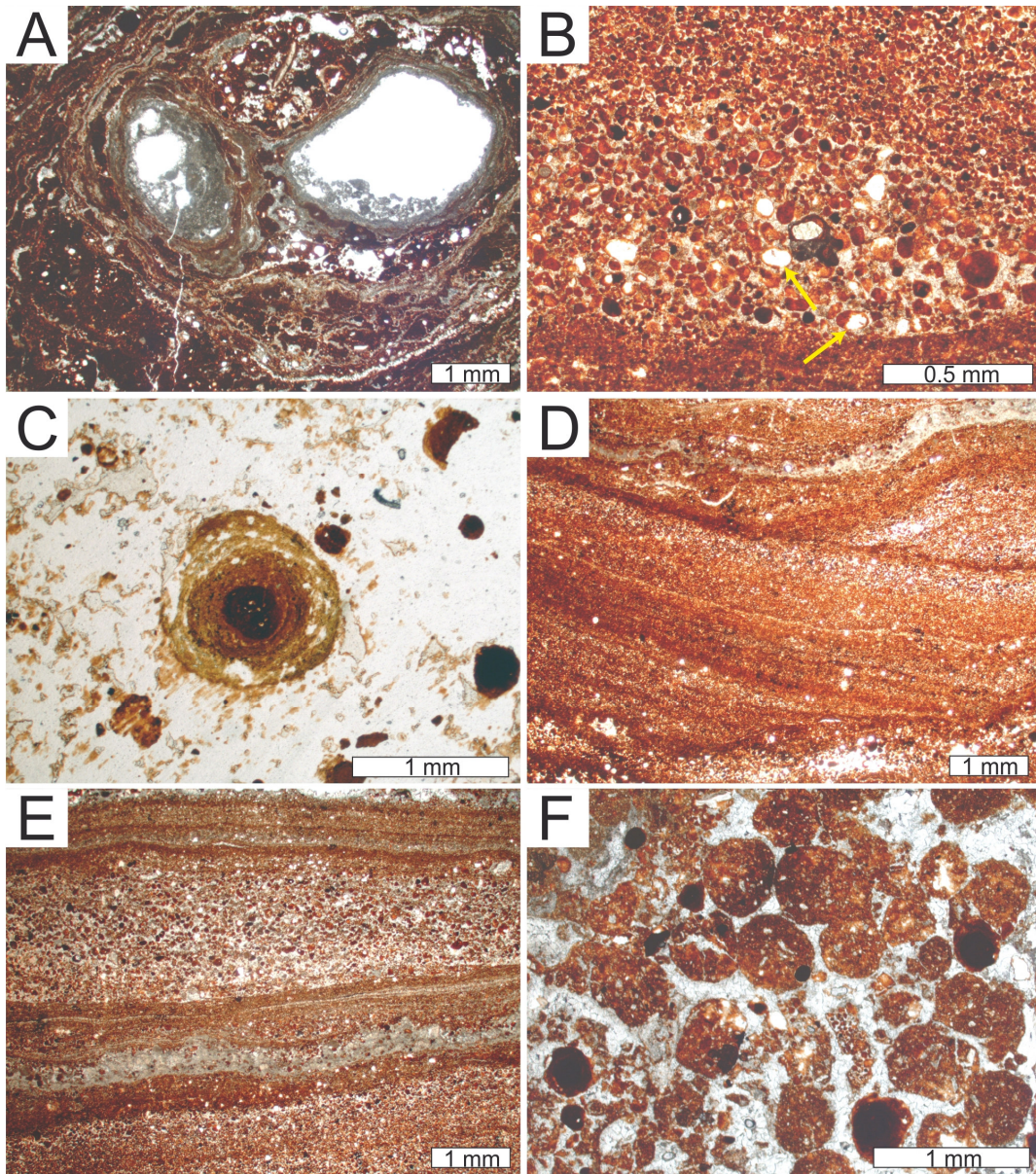
Appendix A: Table A1. Correlation matrix of chemical element contents of bauxites, semi-weathered limestones and bedrock limestones of the Las Mercedes deposit.

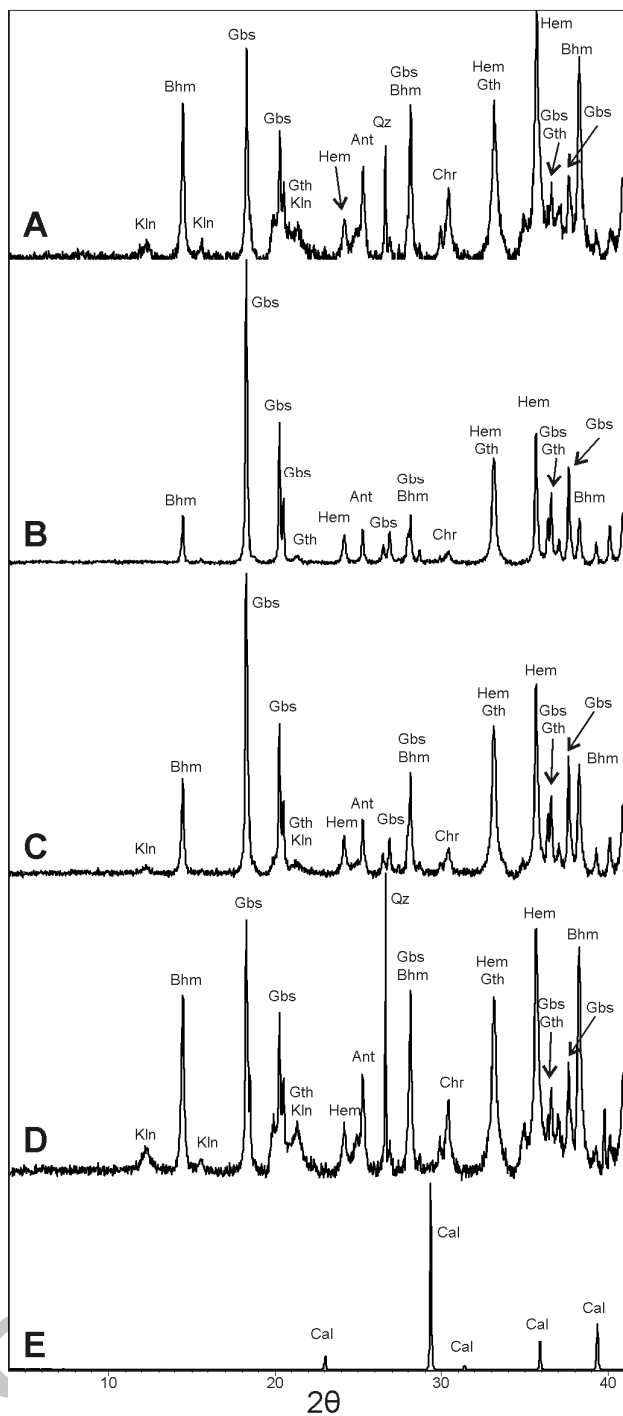


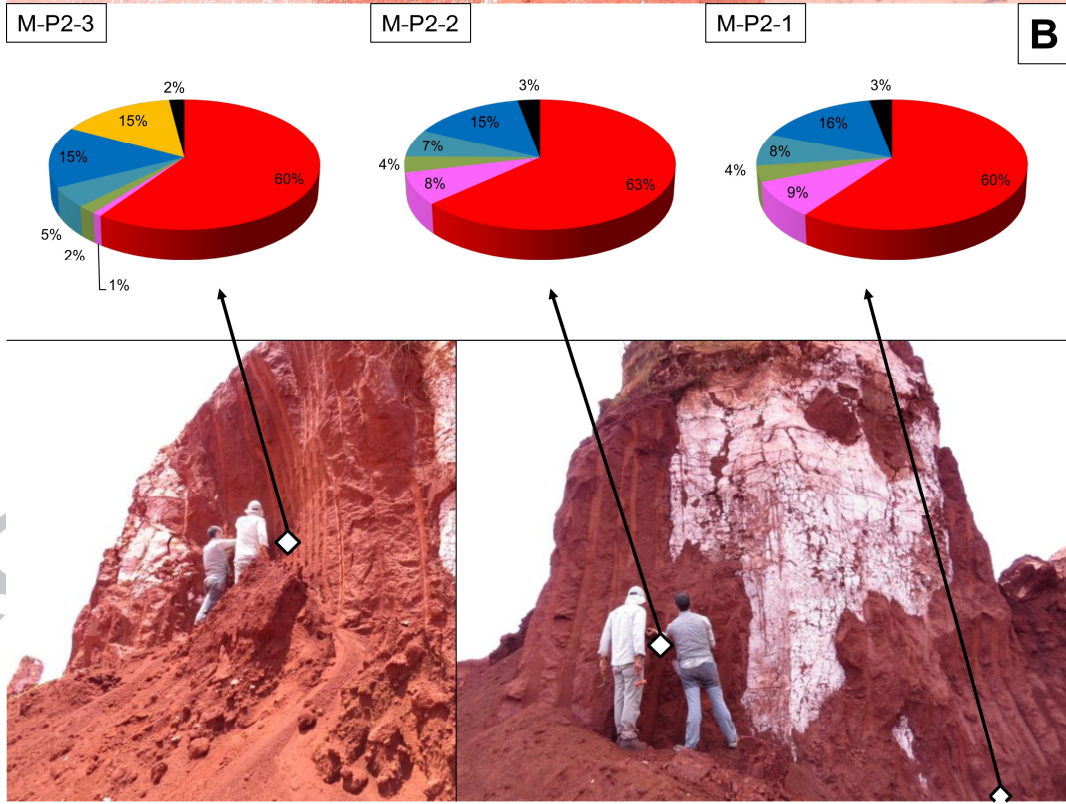
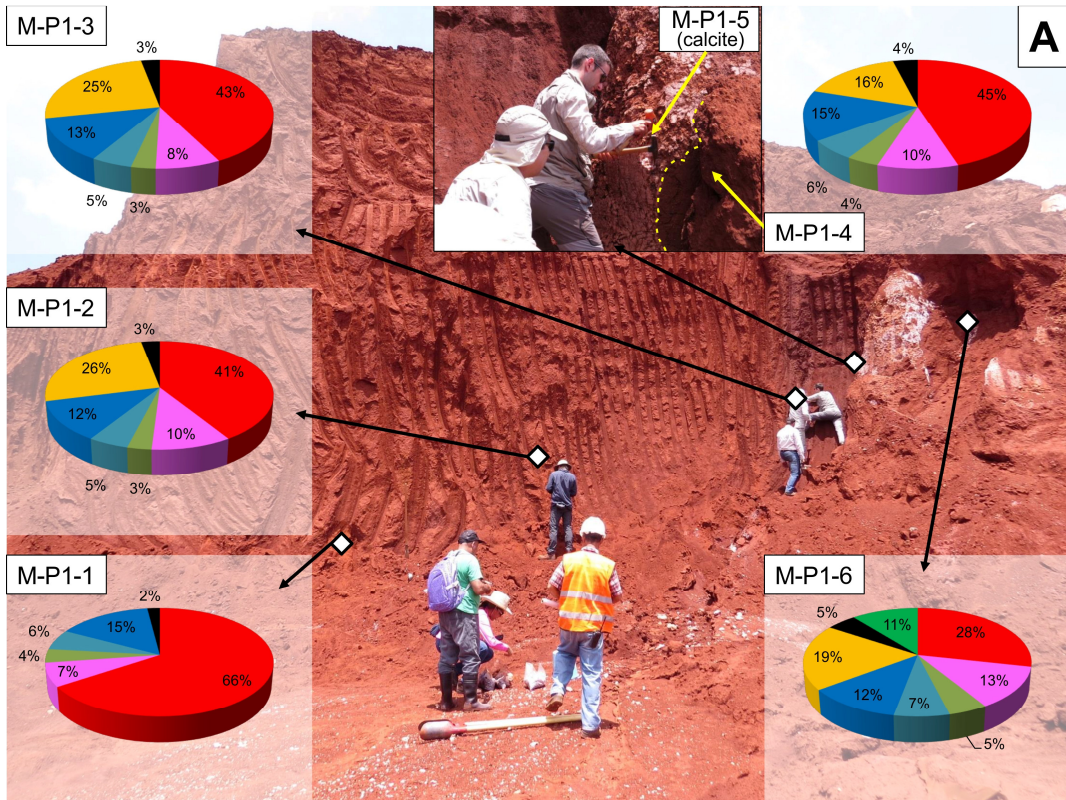


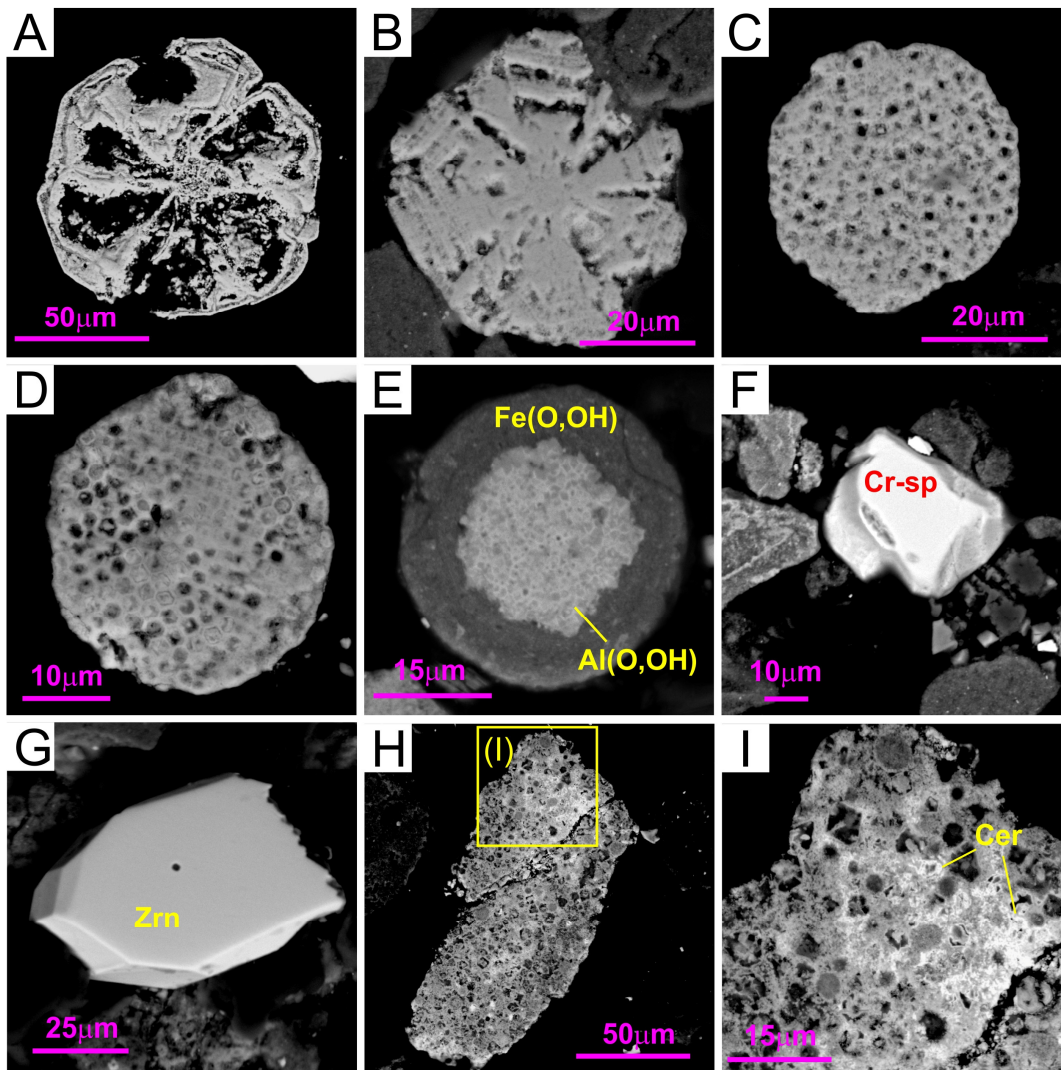


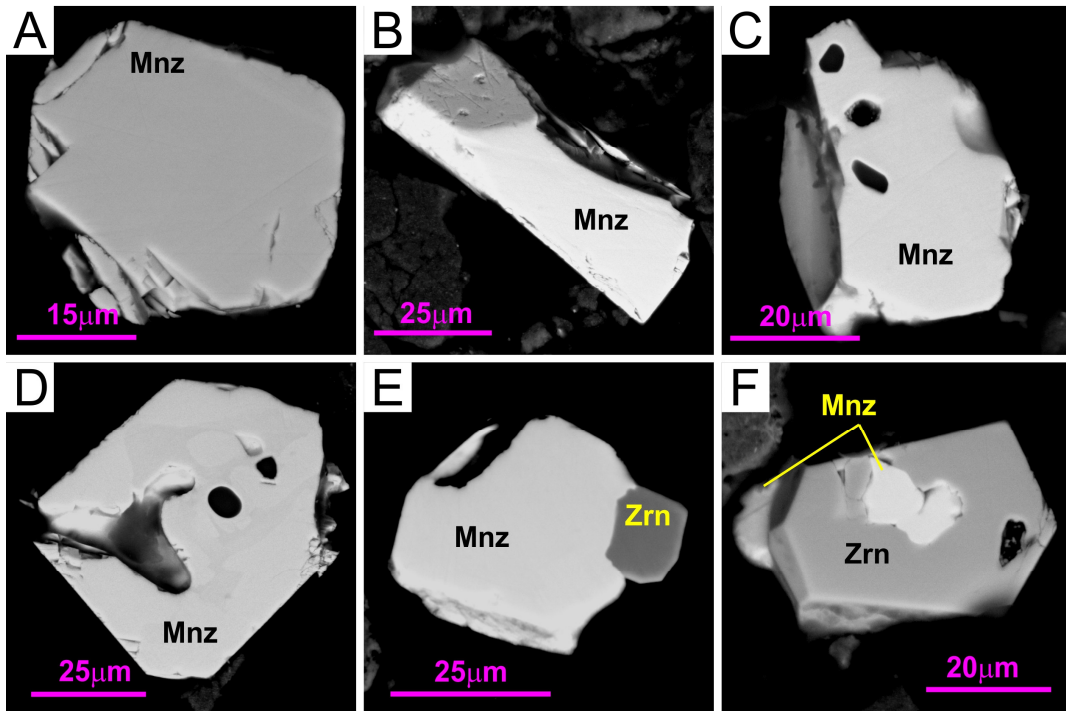


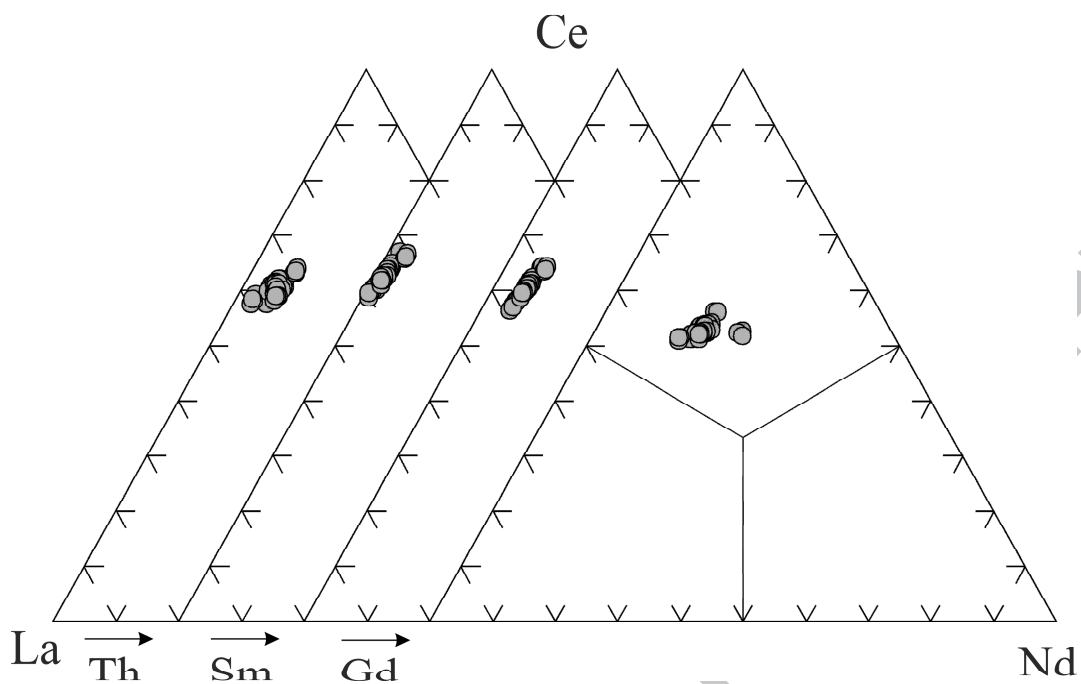




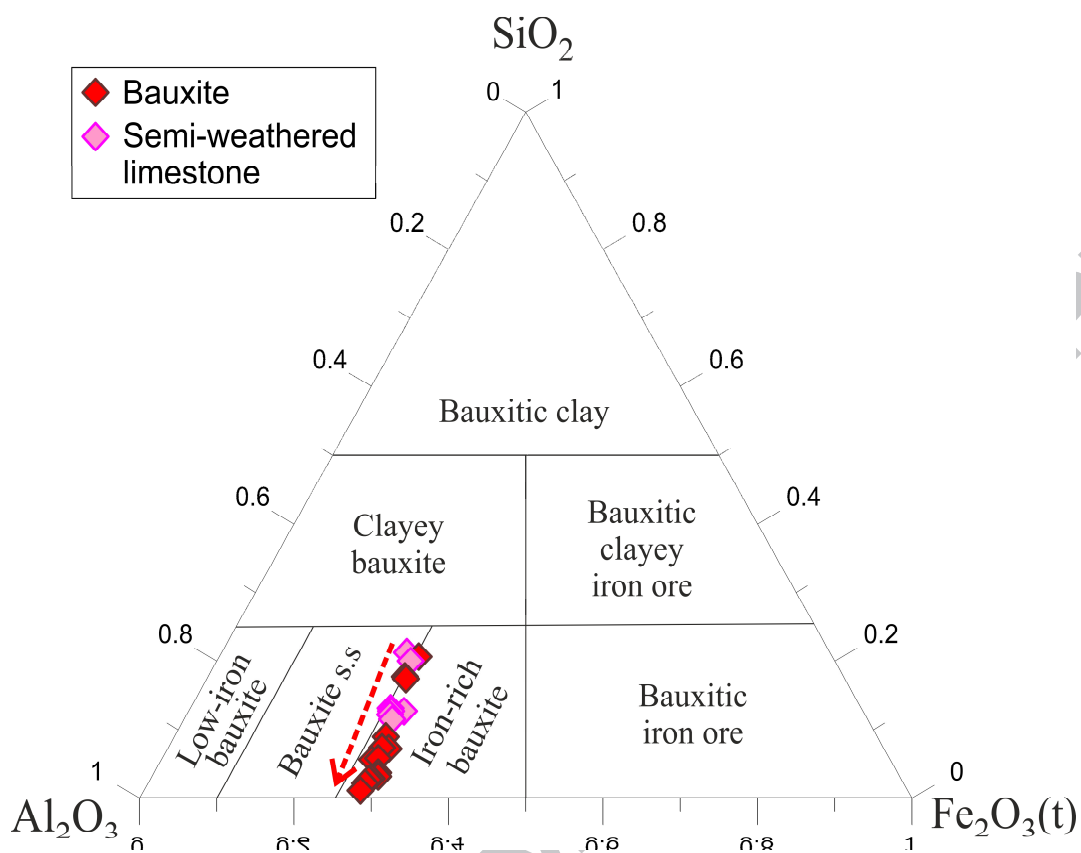


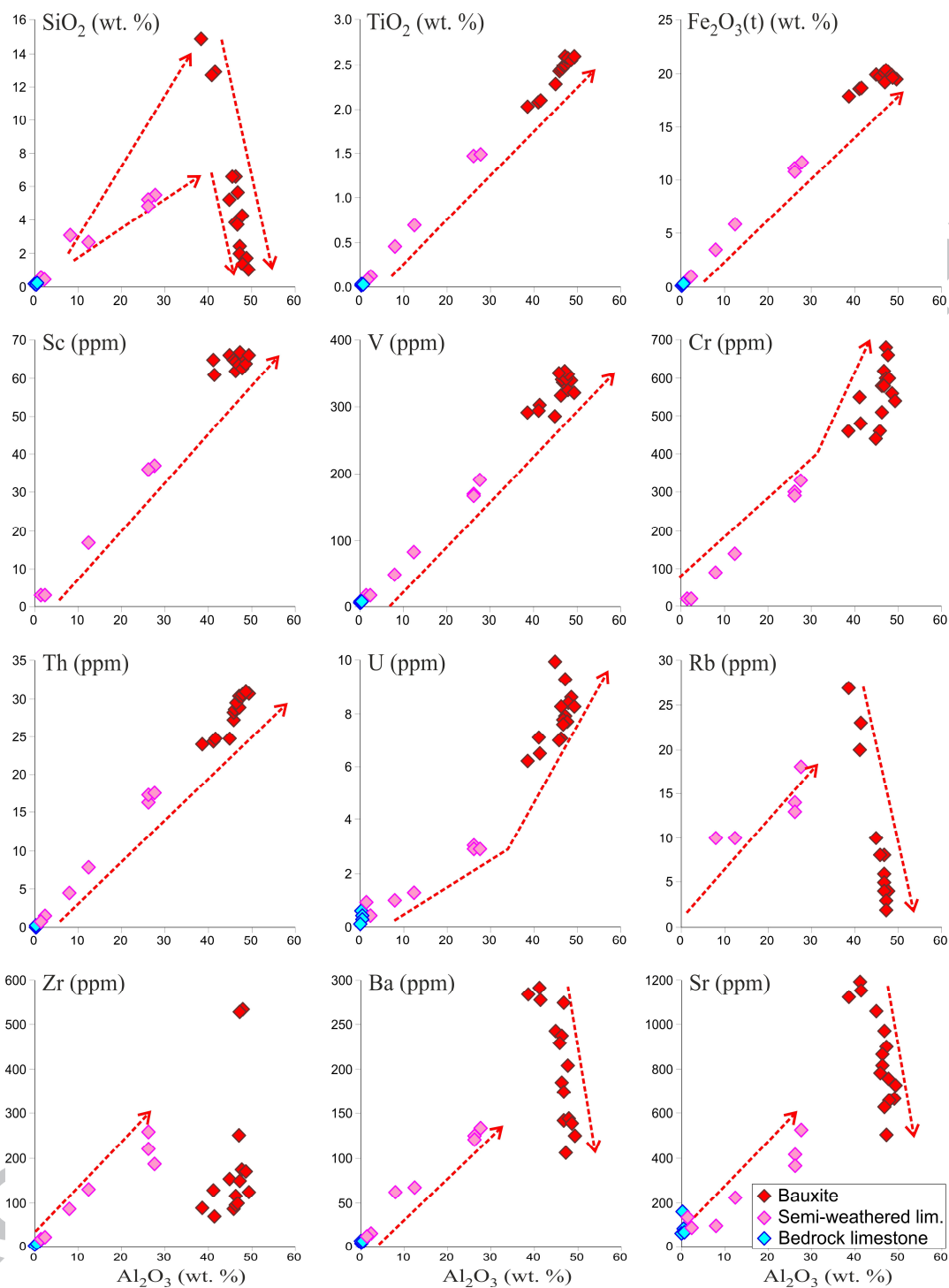


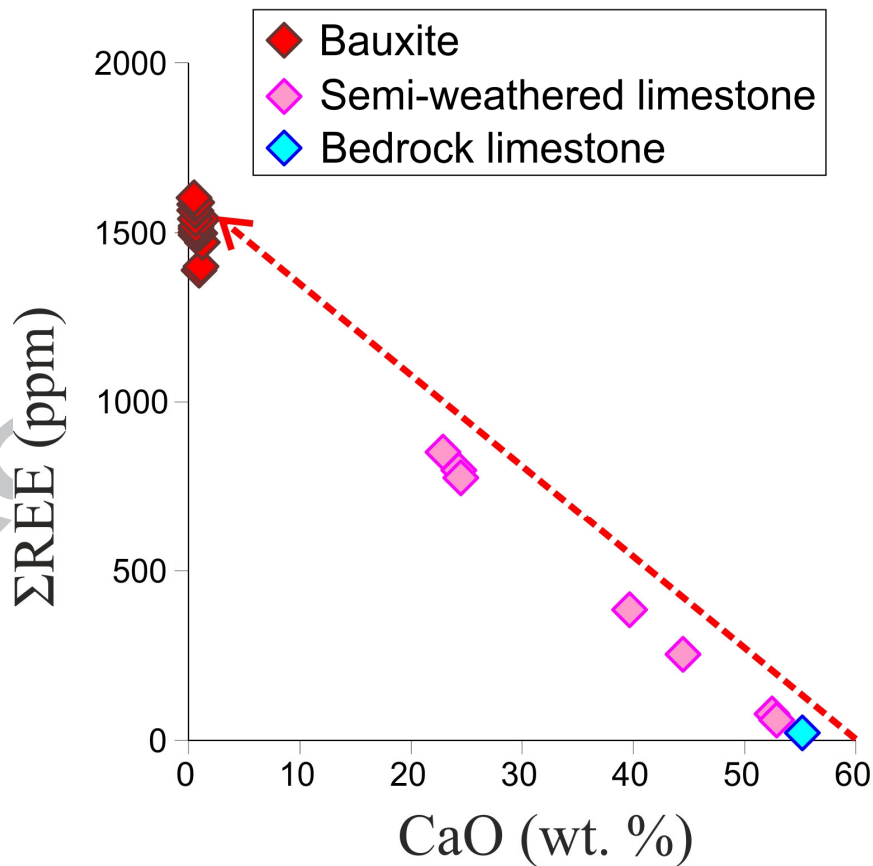
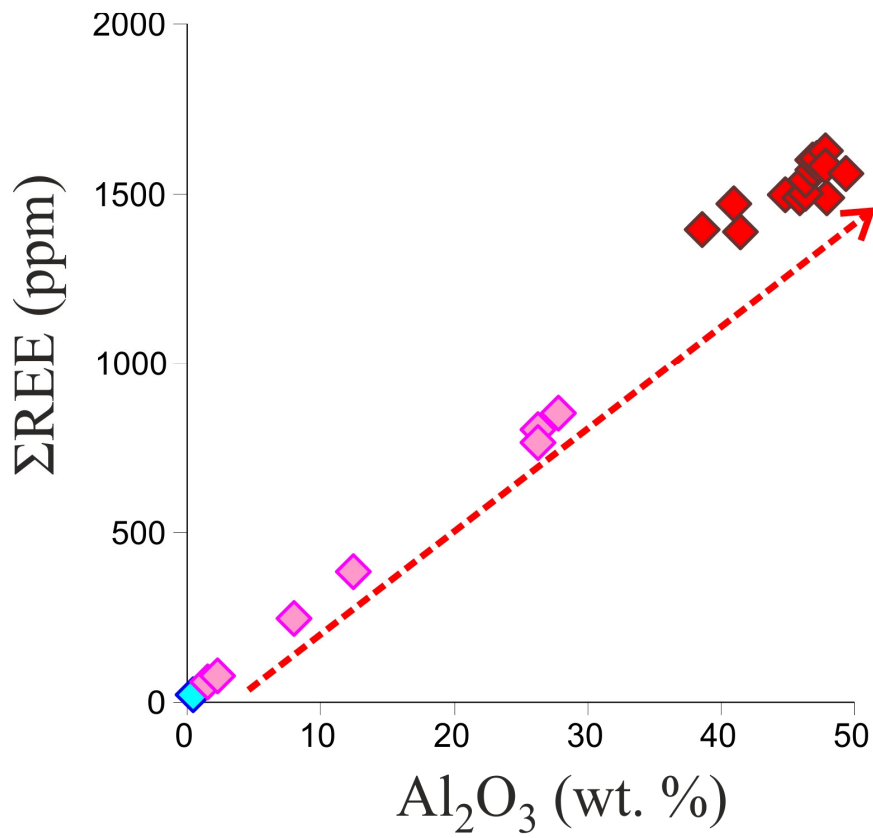


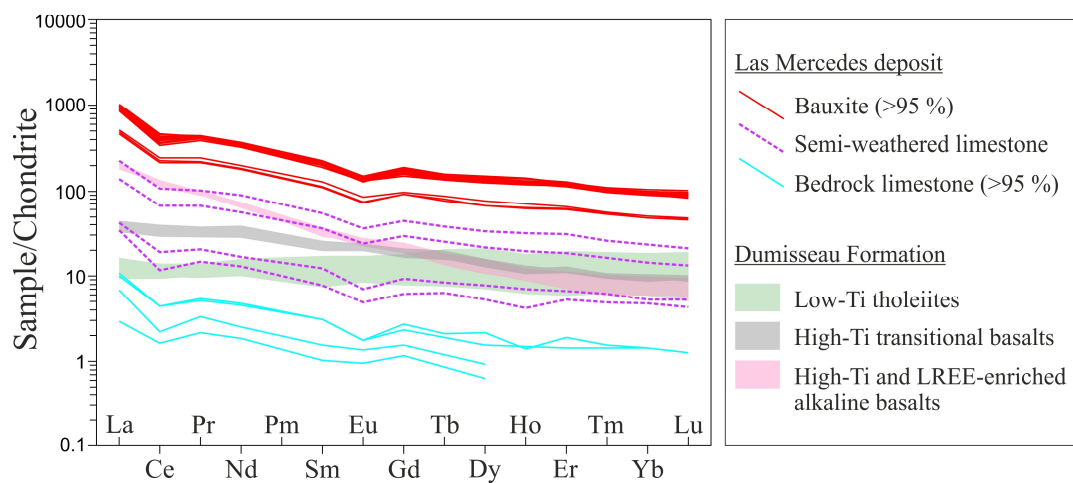


ACCEPTED MANUSCRIPT





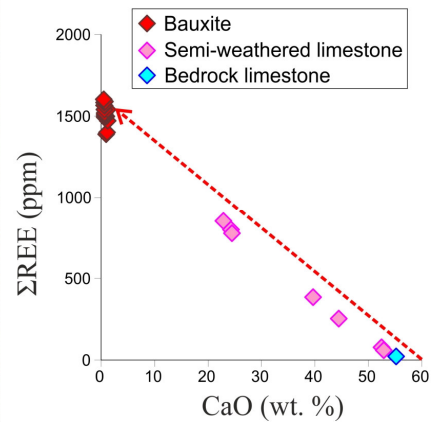
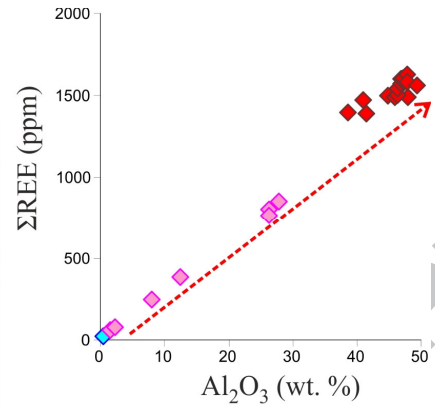




HIGHLIGHTS

- Bauxite deposits may bear important concentrations of REE.
- The Las Mercedes bauxite deposit, Dominican Republic, is currently under production.
- Ore has relatively high and homogeneous REE contents ($\Sigma\text{REE} > 1400$ ppm).
- These concentrations suggest that REE might be benefited as by-product of Al.
- The origin of bauxites in Las Mercedes are most likely lithified bauxites at higher elevations.

ACCEPTED MANUSCRIPT



Anal.no.	30-75- 2_001	30-75- 2_009	30-75- 2_010	30-75- 2_012	30-75- 4_008	30-75- 4_009	30-75- 4_011	30-75- 4_013
P ₂ O ₅ (wt. %)	30.14	29.73	30.18	29.77	29.20	29.36	30.04	29.48
SiO ₂	d.l.	d.l.	0.44	d.l.	0.66	d.l.	0.44	d.l.
CaO	0.95	0.39	0.95	0.96	0.20	0.13	1.00	1.08
BaO	d.l.	d.l.	d.l.	d.l.	d.l.	0.12	d.l.	d.l.
SrO	0.08	d.l.	d.l.	0.08	d.l.	d.l.	d.l.	0.09
UO ₂	d.l.	0.23	d.l.	d.l.	d.l.	0.21	d.l.	d.l.
ThO ₂	3.36	4.22	4.25	4.81	4.83	4.91	4.31	4.22
Ga ₂ O ₃	d.l.							
Y ₂ O ₃	0.35	d.l.						
La ₂ O ₃	17.63	19.45	16.44	16.00	13.79	13.49	16.75	16.39
Ce ₂ O ₃	31.21	30.59	30.68	30.91	29.38	29.37	30.47	31.15
Pr ₂ O ₃	2.86	2.59	2.65	2.67	3.14	3.02	2.68	2.74
Nd ₂ O ₃	10.02	9.35	10.23	10.36	12.97	13.59	10.35	10.43
Sm ₂ O ₃	0.50	0.39	0.60	0.83	1.27	1.39	0.69	0.76
Eu ₂ O ₃	0.50	0.43	0.45	0.53	0.48	0.48	0.47	0.40
Gd ₂ O ₃	2.63	2.72	2.84	2.74	3.14	3.12	2.74	2.78
Tb ₂ O ₃	d.l.							
Dy ₂ O ₃	0.17	0.09	0.16	d.l.	0.37	0.45	0.11	0.16
Ho ₂ O ₃	d.l.	d.l.	d.l.	d.l.	d.l.	0.10	0.23	d.l.
Er ₂ O ₃	d.l.							
Tm ₂ O ₃	d.l.	0.12	0.07	0.21	0.29	0.19	0.12	0.15
Yb ₂ O ₃	d.l.							
Lu ₂ O ₃	d.l.	0.06						
SUM	100.40	100.30	99.93	99.88	99.73	99.93	100.40	99.89
P (<i>a.p.f.u.</i>)	0.997	0.995	0.996	0.995	0.982	0.994	0.991	0.989
Si	0.000	0.000	0.017	-	0.026	-	0.017	-
Sum B	0.997	0.995	1.013	0.995	1.008	0.994	1.008	0.989
Ca	0.040	0.016	0.040	0.041	0.009	0.006	0.042	0.046
Ba	-	-	0.000	-	-	0.002	-	-
Sr	0.002	-	-	0.002	-	-	-	0.002
U	-	0.002	-	-	-	0.002	-	-
Th	0.030	0.038	0.038	0.043	0.044	0.045	0.038	0.038
Ga	-	-	-	-	-	-	-	-
Y	0.007	-	-	-	-	-	-	-
La	0.254	0.283	0.236	0.233	0.202	0.199	0.241	0.240
Ce	0.446	0.443	0.438	0.447	0.427	0.430	0.435	0.452
Pr	0.041	0.037	0.038	0.038	0.045	0.044	0.038	0.040
Nd	0.140	0.132	0.142	0.146	0.184	0.194	0.144	0.148
Sm	0.007	0.005	0.008	0.011	0.017	0.019	0.009	0.010

Eu	0.007	0.006	0.006	0.007	0.007	0.007	0.006	0.005
Gd	0.034	0.036	0.037	0.036	0.041	0.041	0.035	0.037
Tb	-	-	-	-	-	-	-	-
Dy	0.002	0.001	0.002	-	0.005	0.006	0.001	0.002
Ho	-	-	-	-	-	0.001	0.003	-
Er	-	-	-	-	-	-	-	-
Tm	-	0.001	0.001	0.003	0.004	0.002	0.001	0.002
Yb	-	-	-	-	-	-	-	-
Lu	-	-	-	0.000	-	-	-	0.001
Sum A	1.009	1.001	0.985	1.007	0.984	0.997	0.994	1.021

d.l. = below detection limit

Lithology		Bauxite									
Analyte Symbol	D.L.	M-P1-1	M-P1-2	M-P1-3	M-P1-4	M-P1-6	M-P2-1	M-P2-2	M-P2-3	M-P3-2	M-P3-3
SiO ₂ (wt. %)	0.01	1.71	5.65	6.59	6.59	12.72	1.43	1.11	4.24	3.76	3.84
Al ₂ O ₃	0.01	48.69	46.74	46.22	45.86	40.97	47.9	49.34	47.81	46.76	46.31
Fe ₂ O ₃ (T)	0.01	19.72	20.04	19.71	19.69	18.58	19.87	19.53	19.82	19.34	19.6
MnO	0.001	0.594	0.653	0.493	0.514	0.641	0.522	0.593	0.489	0.498	0.555
MgO	0.01	0.07	0.11	0.13	0.13	0.26	0.08	0.07	0.1	0.1	0.1
CaO	0.01	0.29	0.4	0.41	0.41	1.24	0.35	0.39	0.4	0.46	1.09
Na ₂ O	0.01	< 0.01	< 0.01	0.01	0.01	0.04	0.01	< 0.01	< 0.01	< 0.01	< 0.01
K ₂ O	0.01	0.02	0.04	0.06	0.06	0.14	0.02	0.01	0.03	0.03	0.04
TiO ₂	0.001	2.572	2.455	2.423	2.427	2.082	2.612	2.598	2.55	2.526	2.441
P ₂ O ₅	0.01	1.21	1.65	1.42	1.39	2.47	1.13	1.22	1.11	1.04	1.53
LOI		24.51	21.14	21.6	21.56	19.03	25.06	24.75	23	23.67	22.82
Total		99.37	98.89	99.06	98.65	98.18	98.98	99.62	99.56	98.18	98.35
Be (ppm)	1	6	6	6	6	6	7	7	6	7	7
V	5	339	337	342	351	295	326	321	349	352	316
Ba	3	139	275	238	230	292	144	126	203	174	185
Sr	2	667	972	816	782	1195	651	726	756	627	869
Zr	4	170	99	116	85	127	536	123	173	253	95
Cr	20	560	580	510	460	550	600	540	660	620	580
Co	1	78	93	68	67	80	70	68	71	67	75
Ni	20	440	570	420	410	500	400	450	430	400	480
Cu	10	160	210	170	160	250	150	180	150	150	180
Zn	30	250	370	330	320	470	240	280	290	310	320
Ga	1	41	43	41	41	39	41	40	41	41	39
Ge	1	< 1	1	1	< 1	1	< 1	< 1	< 1	< 1	< 1
As	5	40	35	30	34	27	31	38	34	36	37
Rb	2	< 2	6	8	8	20	4	< 2	4	4	5
Nb	1	27	23	22	21	21	50	26	26	31	22
Mo	2	3	3	3	3	2	< 2	3	3	3	3
Ag	0.5	0.6	< 0.5	< 0.5	< 0.5	1.2	2.3	0.7	0.7	0.8	< 0.5
In	0.2	0.4	0.3	0.3	0.3	0.3	0.4	0.5	0.4	0.4	0.4
Sn	1	5	4	4	4	4	7	9	5	5	4
Sb	0.5	2.9	3.1	2.9	3	4	2.7	3.4	2.7	2.5	3.4
Cs	0.5	0.5	1.4	2	2	4	0.6	0.5	1.1	1.1	1.3
Hf	0.2	6.7	4.3	4.9	4	5.1	12.2	5.7	6.6	8.1	4.7
Ta	0.1	1	0.5	0.6	0.4	0.7	2.1	0.9	0.9	1.3	0.8
W	1	3	4	3	3	2	5	4	3	3	3
Tl	0.1	0.2	0.2	0.3	0.3	0.7	0.3	0.2	0.2	0.2	0.2
Pb	5	99	93	84	85	78	75	97	94	95	91
Bi	0.4	1.3	1	0.9	1	0.8	1.4	1.3	1.1	1.1	1.1
Th	0.1	31	28.8	28.2	27.2	24.4	30.7	30.7	30.4	29.5	28.7
U	0.1	8.6	7.8	7.1	7	7.1	8.4	8.3	7.7	7.6	8.3
Sc	1	64	65	65	65	65	63	66	66	64	62

Y	2	365	400	391	388	377	392	377	416	423	390
La	0.1	313	302	282	283	279	273	306	312	302	294
Ce	0.1	361	333	311	308	291	317	345	340	333	330
Pr	0.05	53.8	52.5	50.8	50.4	49.8	49.5	52.3	53.8	52.9	51.7
Nd	0.1	217	215	207	204	202	199	210	219	215	212
Sm	0.1	42.3	42	40.2	40.5	40.8	38.9	41.8	44	42.3	42.3
Eu	0.05	10.5	10.6	9.97	10	10.3	9.43	10.2	11	10.8	10.3
Gd	0.1	45.8	46.2	43.6	41.9	43.3	43.5	43.5	48.7	47	45.3
Tb	0.1	7.2	7.3	6.9	6.7	6.8	6.7	6.7	7.5	7.5	7
Dy	0.1	44.7	45.1	43.1	41.5	42.7	41.3	42.4	47.5	46.5	44.3
Ho	0.1	9.2	9.4	9	8.8	9.3	8.7	9	10.3	10	9.5
Er	0.1	24.9	25.9	25.4	24.4	26.5	23.9	24.6	26.4	27	25.9
Tm	0.05	3.2	3.32	3.31	3.14	3.57	3.1	3.21	3.45	3.43	3.34
Yb	0.1	19.3	19.5	19.4	18.6	21.9	19.3	20	20.6	20.8	19.9
Lu	0.04	2.75	2.91	2.78	2.71	3.26	2.69	2.95	2.9	3.07	2.98
ΣREE		1583.7	1579.7	1510.5	1496.7	1472.2	1491.0	1560.7	1629.2	1608.3	1550.5
ΣLREE		997.6	955.1	901.0	895.9	872.9	886.8	965.3	979.8	956.0	940.3
ΣHREE		157.1	159.6	153.5	147.8	157.3	149.2	152.4	167.4	165.3	158.2
ΣLREE/ΣHREE		6.4	6.0	5.9	6.1	5.5	5.9	6.3	5.9	5.8	5.9
(La/Yb)CN		10.9	10.4	9.8	10.3	8.6	9.5	10.3	10.2	9.8	10.0
(La/Sm)CN		4.7	4.5	4.4	4.4	4.3	4.4	4.6	4.5	4.5	4.4
(Gd/Yb)CN		1.9	1.9	1.8	1.8	1.6	1.8	1.8	1.9	1.8	1.8
Ce/Ce*		0.8	0.8	0.8	0.8	0.8	0.8	0.8	0.8	0.8	0.8
Eu/Eu*		0.7	0.7	0.7	0.7	0.7	0.7	0.7	0.7	0.7	0.7

ΣREE = Sc + Y + Σ(La-Lu); ΣLREE = Σ(La-Eu); ΣHREE = Σ(Gd-Lu); (La/Yb)CN = (La/LaC) / (Yb/YbC); (La/Sm)CN = (La/LaC) / (Sm/SmC)

	SiO ₂	Al ₂ O ₃	Fe ₂ O ₃ (T)	MnO	MgO	CaO	Na ₂ O	K ₂ O	TiO ₂	P ₂ O ₅	Be	V	Ba	Sr	Zr	Cr
SiO ₂	1															
	0.44															
Al ₂ O ₃	831	1														
	207															
Fe ₂ O ₃ (T)	0.50	0.99														
	081	726														
	036	192	1													
MnO	0.56	0.94	0.96													
	699	842	026													
	156	793	749	1												
	-	-	-	-												
MgO	0.83	0.00	0.04	0.14												
	499	646	709	925												
	245	826	369	235	1											
	-	-	-	-	-											
CaO	0.53	0.99	0.99	0.96	0.08											
	749	408	851	520	986											
	156	764	968	813	592	1										
	-	-	-	-	-	-										
Na ₂ O	0.44	0.04	0.07	0.07	0.56	0.09										
	177	471	967	375	108	081										
	418	029	813	478	732	384	1									
	-	-	-	-	-	-	-									
K ₂ O	0.78	0.17	0.21	0.23	0.85	0.24	0.68									
	493	323	914	502	466	757	882									
	563	282	796	945	76	76	118	1								
	-	-	-	-	-	-	-	-								
TiO ₂	0.42	0.99	0.99	0.94	0.01	0.99	0.04	0.16								
	844	884	459	328	748	060	558	327								
	135	036	772	423	611	635	07	856	1							
	-	-	-	-	-	-	-	-	-							
P ₂ O ₅	0.80	0.78	0.81	0.85	0.43	0.83	0.28	0.52	0.75							
	644	073	833	607	721	543	616	691	759							
	331	415	243	799	911	994	584	734	817	1						
	-	-	-	-	-	-	-	-	-	-						
Be	0.43	0.97	0.97	0.93	0.01	0.96	0.13	0.22	0.96	0.80						
	721	106	558	897	326	994	244	489	996	789						
	622	001	85	346	123	245	679	769	983	479	1					
	-	-	-	-	-	-	-	-	-	-	-					
V	0.47	0.99	0.99	0.95	0.00	0.99	0.02	0.16	0.99	0.77	0.95					
	479	501	435	035	965	279	822	060	362	988	649					
	023	11	01	87	575	937	33	668	591	461	556	1				
	-	-	-	-	-	-	-	-	-	-	-	-				
Ba	0.83	0.81	0.85	0.84	0.42	0.86	0.21	0.52	0.80	0.93	0.79	0.83				
	148	950	098	650	243	702	205	623	143	933	092	279				
	437	705	976	13	582	263	247	095	279	846	05	631	1			

	0.75	0.85	0.88	0.89	0.33	-	0.22	0.42	0.83	0.97	0.85	0.85	0.95				
	445	602	436	214	118	641	834	625	556	585	459	938	420				
Sr	213	777	33	451	931	419	826	663	622	331	393	95	563	1			
	-				-	-											
	0.01	0.53	0.51	0.49	0.11	0.50	0.06	0.04	0.56	0.17	0.56	0.51	0.19	0.19			
	376	099	739	620	965	391	389	110	169	167	806	003	738	968			
Zr	561	698	941	756	511	871	291	179	901	179	005	119	672	264	1		
	0.42	0.98	0.97	0.94	0.02	0.97	0.04	0.12	0.98	0.73	0.95	0.98	0.77	0.82	0.58		
	064	173	849	540	310	492	259	098	430	593	140	261	982	157	907		
Cr	966	123	955	272	882	292	382	779	773	138	638	512	49	292	194	1	
	0.53	0.96	0.97	0.99	0.08	0.97	0.05	0.19	0.95	0.84	0.94	0.96	0.85	0.90	0.48	0.96	
	730	445	453	177	847	561	102	157	923	685	700	870	667	016	573	401	
Co	566	216	39	114	549	642	789	831	736	252	417	953	519	771	941	944	
	0.50	0.95	0.96	0.98	0.06	0.96	0.11	0.21	0.95	0.84	0.96	0.95	0.83	0.89	0.49	0.95	
	628	706	835	160	704	528	990	074	271	220	682	421	241	120	788	473	
Ni	865	399	423	59	77	964	155	553	671	285	375	129	204	624	872	483	
	0.71	0.90	0.92	0.95	0.31	0.93	0.25	0.44	0.88	0.95	0.92	0.89	0.92	0.96	0.37	0.87	
	393	263	777	538	662	797	054	799	971	900	077	822	794	573	081	591	
Cu	455	725	215	778	552	567	695	067	041	041	223	804	069	703	737	221	
	0.78	0.87	0.90	0.94	0.39	0.91	0.20	0.43	0.86	0.94	0.86	0.88	0.94	0.95	0.33	0.86	
	662	319	207	612	251	851	385	955	082	304	771	691	585	628	116	216	
Zn	093	737	793	955	063	333	223	946	575	686	031	14	28	254	387	094	
	0.53	0.99	0.99	0.95	0.08	0.99	0.07	0.23	0.99	0.81	0.95	0.99	0.86	0.88	0.51	0.97	
	000	322	562	927	156	707	476	152	135	089	562	508	183	160	106	821	
Ga	642	047	789	467	326	615	088	359	151	929	428	286	944	417	923	804	
	0.34	0.97	0.97	0.92	0.08	0.96	0.05	0.10	0.98	0.70	0.95	0.97	0.72	0.78	0.55	0.97	
	907	897	091	903	297	309	237	258	283	065	726	341	843	725	090	399	
As	687	173	652	967	005	082	959	047	484	085	215	203	714	737	424	551	
	0.91	0.22	0.27	0.32	0.94	0.31	0.61	0.94	0.21	0.61	0.24	0.23	0.62	0.52	0.00	0.18	
	039	408	593	778	032	262	890	934	100	542	632	060	005	950	941	960	
Rb	298	22	701	079	498	661	326	126	189	727	602	372	615	176	456	343	
	0.25	0.86	0.85	0.77	0.03	0.84	0.17	0.16	0.88	0.53	0.85	0.84	0.57	0.60	0.82	0.87	
	285	240	088	147	940	172	215	601	020	445	978	082	817	553	784	242	
Nb	438	947	941	065	235	317	552	639	886	018	313	781	446	606	28	573	
	0.67	0.91	0.93	0.95	0.25	0.94	0.16	0.33	0.89	0.94	0.91	0.91	0.90	0.97	0.30	0.88	
	366	254	269	074	217	246	549	204	724	510	379	266	421	496	912	359	
Sb	875	154	954	825	783	209	514	407	085	696	397	582	808	238	925	779	
	0.98	0.37	0.43	0.49	0.89	0.46	0.53	0.85	0.36	0.74	0.38	0.39	0.75	0.68	0.00	0.34	
	065	865	143	162	066	783	167	899	165	781	716	679	553	789	683	698	
Cs	745	226	597	893	642	108	543	073	17	679	08	25	345	621	143	991	

		0.18	0.80	0.79	0.69	-	-	0.13	0.15	0.82	0.45	0.80	0.78	0.50	0.52	0.86	0.82	0
	Hf	549	728	054	702	336	090	798	231	669	363	441	265	347	251	825	565	1
		685	929	988	843	397	766	355	949	403	869	301	412	955	859	032	331	3
		0.08	0.72	0.70	0.62	0.11	0.69	0.14	0.08	0.74	0.38	0.75	0.69	0.38	0.43	0.88	0.75	0
	Ta	873	521	869	848	250	727	735	274	731	622	326	226	730	565	347	168	6
		175	526	152	868	349	79	847	101	14	514	361	94	357	751	324	316	6
		0.42	0.98	0.98	0.95	0.03	0.98	0.00	0.10	0.98	0.76	0.95	0.99	0.79	0.84	0.49	0.98	0
	Pb	794	904	541	793	205	247	117	821	777	188	626	044	524	300	145	359	2
		543	538	661	511	776	154	999	379	643	328	269	466	293	135	347	695	0
		0.42	0.99	0.99	0.94	0.01	0.98	0.03	0.15	0.99	0.74	0.96	0.99	0.79	0.83	0.56	0.98	0
	Th	650	754	212	304	678	876	307	355	894	939	197	312	604	124	245	689	9
		045	545	528	811	686	584	906	201	638	473	272	294	477	19	913	112	3
		0.36	0.96	0.96	0.93	0.10	0.96	0.00	0.07	0.96	0.79	0.97	0.95	0.77	0.85	0.47	0.94	0
	U	820	896	827	321	626	132	101	069	299	722	056	886	510	784	714	907	3
		804	286	025	043	479	217	413	743	846	081	673	001	702	333	269	828	5
		0.51	0.99	0.99	0.95	0.05	0.99	0.09	0.22	0.99	0.82	0.97	0.99	0.85	0.89	0.49	0.97	0
	Sc	466	556	878	992	573	839	004	494	174	869	311	314	977	339	711	581	3
		388	84	695	723	328	906	19	516	074	004	094	237	769	353	554	626	6
		0.49	0.99	0.99	0.95	0.02	0.99	0.05	0.17	0.98	0.82	0.97	0.99	0.85	0.89	0.48	0.97	0
	Y	627	163	504	467	548	409	132	927	764	191	048	340	419	051	762	856	3
		941	196	248	142	982	423	39	644	439	736	02	829	023	095	899	273	6
		0.47	0.99	0.99	0.96	0.01	0.99	0.04	0.16	0.99	0.80	0.96	0.99	0.82	0.87	0.49	0.98	0
	La	230	506	525	512	163	382	500	342	255	033	809	504	878	248	964	561	9
		707	429	833	796	804	923	684	655	244	427	155	053	697	003	487	94	9
		0.42	0.99	0.99	0.95	0.02	0.98	0.04	0.14	0.99	0.75	0.96	0.99	0.79	0.83	0.54	0.98	0
	Ce	076	605	214	430	997	787	259	286	656	879	853	231	259	669	718	889	9
		916	676	861	425	67	697	473	451	91	8	271	17	405	398	476	962	2
		0.49	0.99	0.99	0.96	0.02	0.99	0.05	0.19	0.99	0.81	0.96	0.99	0.84	0.88	0.49	0.98	0
	Pr	272	671	772	111	950	711	262	195	345	200	814	610	620	204	698	244	5
		094	639	42	834	559	747	612	061	995	411	22	375	825	521	749	103	2
		0.49	0.99	0.99	0.96	0.02	0.99	0.05	0.19	0.99	0.81	0.97	0.99	0.84	0.88	0.49	0.98	0
	Nd	270	640	804	193	938	703	719	190	306	452	036	578	694	403	499	263	7
		08	536	797	595	804	129	01	91	229	98	93	995	212	246	89	88	9
		0.49	0.99	0.99	0.95	0.03	0.99	0.07	0.20	0.99	0.81	0.96	0.99	0.84	0.88	0.49	0.98	0
	Sm	890	565	712	920	743	661	172	106	257	285	741	525	787	419	150	344	4
		853	495	923	436	982	513	025	842	659	925	351	324	001	007	566	099	7
		0.51	0.99	0.99	0.95	0.05	0.99	0.07	0.21	0.98	0.82	0.96	0.99	0.86	0.89	0.48	0.98	0
	Eu	668	387	672	972	453	692	415	907	098	570	725	387	116	354	020	005	5
		815	007	205	994	789	932	669	437	978	373	923	105	303	136	368	944	9

